Long-term estimation of diurnal vertical $\mathbf{E}\times\mathbf{B}$ drift velocities using C/NOFS and ground-based magnetometer observations

John Bosco Habarulema[1,2], Makhosonke B. Dubazane[1,2], Zama T Katamzi-Joseph[1,2], Endawoke Yizengaw[3], Mark B. Moldwin[4] and Jean Claude Uwamahoro[1,2]

[1]South African National Space Agency (SANSA), Space Science , P.O Box 32, Hermanus 7200, South Africa.
[2]Department of Physics and Electronics, Rhodes University, 6140 Grahamstown, South Africa.
[3]Institute for Scientific Research, Boston College, USA.
[4]Department of Climate and Space Sciences and Engineering, University of Michigan, Ann Arbor, Michigan, USA.

Key Points:

- Development of a relationship between C/NOFS vertical $\mathbf{E}\times\mathbf{B}$ drifts and magnetometer derived EEJ during 2008-2014.
- At least 80% of the differences between observed and derived $\mathbf{E}\times\mathbf{B}$ lie within ±5 m/s when validated with radar observations
- The developed relationship is applicable during quiet and disturbed conditions

Corresponding author: John Bosco Habarulema, jhabarulema@sansa.org.za

Abstract

We report on the development of a new mathematical expression to estimate local day-time (0700-1700 LT) vertical $\mathbf{E}\times\mathbf{B}$ drift in low latitudes using a combination of ground-based magnetometer measurements and Communications and Navigation Outage Forecasting System (C/NOFS) satellite observations. The expression was developed over Jicamarca (11.8°S, 77.2°W; 0.8°N geomagnetic) and validated with Jicamarca Unattended Long-Term studies of the Ionosphere and Atmosphere (JULIA) mode and incoherent scatter radar (ISR) measurements during the period 2008-2014. The obtained correlation coefficient (R) values computed using observed and derived vertical $\mathbf{E}\times\mathbf{B}$ drift velocities are 0.79 and 0.84 for ISR and JULIA respectively when data are available during 2008-2014. Storm-time comparison between observed and derived vertical $\mathbf{E}\times\mathbf{B}$ drift velocities agreed well with R of 0.92 and 0.87 during 05-08 August 2011 and 08-11 March 2012 geomagnetic storm periods for ISR and JULIA observations respectively. Overall, we found that the developed expression is applicable in estimating vertical $\mathbf{E}\times\mathbf{B}$ drift response during quiet and geomagnetic storm periods. Based on these findings, we suggest that it is possible to develop accurate day-time global vertical $\mathbf{E}\times\mathbf{B}$ drift model over the equatorial latitude regions using inexpensive magnetometer observations and available satellite data.

1 Introduction

The importance of zonal electric fields in influencing plasma electrodynamics in low or equatorial latitude regions is well known [e.g., *Scherliess and Fejer*, 1997, 1999; *Patra et al.*, 2004; *Fejer et al.*, 2008; *Huang et al.*, 2005; *Patra et al.*, 2014] and include controlling the extent of the equatorial ionisation anomaly and vertical coupling between the low and high altitude ionospheric layers and associated physical processes. However, in general, electric field data remain sparse in most longitude sectors. Traditionally, day-to-day variability studies of equatorial vertical $\mathbf{E}\times\mathbf{B}$ drifts at all local times were possible using the Jicamarca Incoherent Scatter Radar (ISR). The evidence that 150 km echoes are a proxy of F2-region vertical $\mathbf{E}\times\mathbf{B}$ drifts [e.g., *Kudeki and Fawcett*, 1993; *Chau and Woodman*, 2004] has made it possible to study changes of vertical $\mathbf{E}\times\mathbf{B}$ drifts in other longitude sectors during local daytime [*Patra and Rao*, 2006; *Patra et al.*, 2008]. Although there have been deployment of back scatter 150 km echo radars that have filled data-gaps in different longitude sectors such as India and Indonesia [*Patra and Rao*, 2006; *Patra* *et al.*, 2008, 2012, 2014], there is still limited vertical $\mathbf{E} \times \mathbf{B}$ drift observations in other regions hindering accurate understanding of the global ionospheric plasma dynamics. It therefore still remains necessary to explore different techniques or approaches that can improve data coverage both in time resolution domain and in different longitude sectors. In this regard, satellite data provides the necessary global coverage, but are non-continous over particular longitude sectors and local times and are hence more appropriate for developing climatological models. Logistically, it is almost impossible to deploy radars at all longitude sectors due to the huge acquisition and operational costs. In an effort to increase continous vertical $\mathbf{E} \times \mathbf{B}$ drift data coverage in low/equatorial latitudes, we propose a simple mathematical approach based on simultaneous consideration of ground-based magnetometer and Communications and Navigation Outage Forecasting System (C/NOFS) satellite data. The first challenge with this is how to validate the proposed approach since vertical $\mathbf{E} \times \mathbf{B}$ drift data is scarce in many longitude sectors. For the beginning, this is best done over a location or longitude sector with extended vertical $\mathbf{E} \times \mathbf{B}$ drift observational data, which makes Jicamarca (11.8°S, 77.2°W; 0.8°N geomagnetic) an excellent choice for this study. The developed approach can then be transferable to other longitude sectors with a particular level of confidence. We have developed a simple expression relating daytime equatorial electrojet (EEJ) estimated from magnetometer measurements (ΔH) using the differential method [e.g., *Rastogi and Klobuchar*, 1990; *Anderson et al.*, 2002, 2004] and C/NOFS vertical component of the ion plasma drift observations over Jicamarca during 2008-2014. These two datasets can be related based on previous findings that ground-based magnetometer derived EEJ approximates daytime changes in the vertical component of the phase velocity of irregularities near 150 km [e.g., *Chau and Woodman*, 2004; *Anderson et al.*, 2004] which correspond to the vertical ion drift and thus the zonal electric field in equatorial regions. The developed expression was validated with Jicamarca ISR's vertical $\mathbf{E} \times \mathbf{B}$ drift and Jicamarca Unattended Long-Term studies of the Ionosphere and Atmosphere (JULIA) system data, including separate treatment of different geophysical conditions. We wish to state that it has been shown previously that JULIA vertical $\mathbf{E} \times \mathbf{B}$ drift data correlate well with EEJ [e.g., *Anderson et al.*, 2004] and have high agreement with ISR vertical $\mathbf{E} \times \mathbf{B}$ drift observations [*Kudeki and Fawcett*, 1993; *Chau and Woodman*, 2004]. A clear historical perspective linking 150 km echo Doppler velocities to equatorial vertical drifts along with relevant references has been presented in *Rodrigues et al.* [2015]. Ground-based magnetometer data have advantage of being continuous with high temporal resolution and are available in a number of longitude sectors, thus increasing the probability of getting coincidental observations when the satellite is within the vicinity of the magnetometer location. It is established that the difference between horizontal components of the Earth's magnetic field observations (ΔH) from magnetometer locations at the equator and about $6^\circ - 9^\circ$ away from the equator is a proxy of EEJ which has a linear relationship with vertical $\mathbf{E}\times\mathbf{B}$ drift [*Anderson et al.*, 2002, 2004; *Yizengaw et al.*, 2014] during local daytime. Therefore the development of a mathematical relationship between C/NOFS vertical ion plasma drift and ΔH has the potential to provide high temporal resolution vertical $\mathbf{E}\times\mathbf{B}$ databases in longitude sectors where low latitude magnetometers exist. This would in turn contribute to formulation of empirical models in equatorial latitudes as well as performing extended day-to-day vertical drift variability on a long-term basis by utilising the extended magnetometer network consisting of pairs that satisfy the criteria for estimating EEJ [e.g., *Yizengaw and Moldwin*, 2009]. Although the approach based on magnetometer observations is valid during local daytime, it may be possible in future to develop $\mathbf{E}\times\mathbf{B}$ drift models covering all times by combining vertical $\mathbf{E}\times\mathbf{B}$ drift data estimated from daytime magnetometer ΔH and night-time satellite observations.

2 Data sources and method

The Ion Velocity Meter (IVM), one of the instruments of the Coupled Ion Neutral Dynamics Investigation (CINDI) package onboard C/NOFS satellite provides in situ observations of equatorial meridional/vertical component of the ion plasma drift [e.g., *Stoneback et al.*, 2011, 2012; *Yizengaw et al.*, 2014] that are used in this study. C/NOFS satellite which was launched in April 2008 in a 13° inclination orbit had initial perigee and apogee at 400 km and 850 km respectively [*Stoneback et al.*, 2011]. The IVM instrument provides vertical ion plasma drift, ion composition and temperature. Detailed information about the instrument calibration for ion plasma drift measurements can be found in *Stoneback et al.* [2012]. The other instrument of CINDI is the neutral wind meter that gives neutral velocity and density observations. In our analysis, we limited C/NOFS vertical ion plasma drift (equivalent to vertical $\mathbf{E}\times\mathbf{B}$ drift at about 400 km) observations within ±4 degrees latitude from the geomagnetic equator based on the fact that the EEJ is a strip of enhanced current within ±3° from the dip equator. Also a study by *Manoj et al.* [2006] showed that the correlation between EEJ derived from ground-based magnetometer data and CHAMP satellite observations deteoriated beyond ±4° from the geomagnetic equator. The longitudinal consideration was limited within 77.2°W±8° to ensure that the local time did not change considerably, while the altitude range was 400-550 km which has been used in several investigations [e.g., *Stoneback et al.*, 2011; *Yizengaw et al.*, 2014; *Rodrigues et al.*, 2015]. From now onwards and for convenience purposes, there may be instances where C/NOFS vertical ion plasma drift is simply referred to as C/NOFS vertical $\mathbf{E} \times \mathbf{B}$ drift, especially during the comparison with ISR and JULIA measurements. The outliers in C/NOFS vertical $\mathbf{E} \times \mathbf{B}$ data were removed per satellite pass (within our defined latitude/longitude and altitude grid) using the median filtering technique centered at determining the median and median absolute deviation. The scaled median deviation (δ) was determined following a procedure in *Huber* [1981]; *Huber and Ronchetti* [2009]; *Lomidze et al.* [2018] as $\delta = b \times \text{median}(|y_i - \text{median}(y_i)|)$, where the constant $b = 1.4826$ is associated with data exhibiting normal distribution [e.g., *Rousseeuw and Croux*, 1993; *Leys et al.*, 2013] and y_i is the number of observations, in this case, per satellite pass within the defined spatial/altitude resolution. Therefore values outside the range; median ± 2.5δ (per satellite pass) were eliminated from further analysis. In total, the combination of median and scaled median absolute deviation removed 2.82% of C/NOFS vertical ion drift as outliers which did not exhibit regular trend in their diurnal temporal variability.

The EEJ was determined from horizontal component of the Earth's magnetic field using a pair of magnetometer stations; Jicamarca (11.8°S, 77.2°W; 0.8°N geomagnetic) and Piura (5.2°S, 80.6°W; 6.8°N geomagnetic). Differencing H-component (to give ΔH) using magnetometer data from a station located at the equator and another one away from the equator by $6° - 9°$ is a widely accepted method of determining EEJ and or vertical $\mathbf{E} \times \mathbf{B}$ drift [*Rastogi and Klobuchar*, 1990; *Anderson et al.*, 2002, 2004; *Yizengaw et al.*, 2011, 2012] during local daytime. The reader is referred to *Anderson et al.* [2002, 2004]; *Yizengaw et al.* [2012] for a detailed description of the method.

Figure 1 shows (a) the location of Jicamarca and Piura magnetometer stations (red dots) along with the spatial coverage considered for C/NOFS vertical ion drifts (enclosed in blue dashed lines) around Jicamarca, (b) daytime H (nT) after removing the background H value by subtracting the average nighttime baseline value between 2300-0300 local time [*Yizengaw et al.*, 2014] over Jicamarca (black curve) and Piura (blue curve) for 08 January 2011, and (c) daytime ΔH (nT) obtained using data in (b) as well as available C/NOFS vertical ion drift (m/s) (plotted as black dots) on 08 January 2011. Figure 1(c) shows that for most of the time when data are available, C/NOFS vertical ion plasma drift and magnetometer ΔH agree even in revealing downward vertical drifts manifesting as negative values in the observations. There were considerable instances with negative values of ΔH and C/NOFS vertical ion drift during our period of study as we will show later in the next section. It has long been established that counter-electrojet (CEJ) occurs during local daytime in low solar activity conditions [*Rastogi*, 1974]. A recent longitudinal study over the African, South American and Phillipine regions during 2009 showed that there were occurrences of CEJ sometimes in local morning and especially in later afternoon [*Rabiu et al.*, 2017]. Some of the mechanisms associated with CEJ include vertical upward winds in equatorial regions [e.g., *Raghavarao and Anandarao*, 1980] and Sudden Stratospheric Warming (SSW) driven dynamo processes [*Vineeth et al.*, 2009]. As a result of the prolonged solar minimum that caused complexities in ionospheric changes especially during 2008-2011 [*Chen et al.*, 2011; *Perna and Pezzopane*, 2016], our subsequent analysis and statistics involve significant CEJ durations when ΔH and C/NOFS vertical ion plasma drifts were negative.

3 Relationship between C/NOFS vertical ion plasma drift and magnetometer observations

Selecting C/NOFS vertical ion plasma (or simply vertical $\mathbf{E} \times \mathbf{B}$) drift data and ΔH at times when both datasets are available within 2008-2014 yields a dataset that can be used to develop a mathematical relationship between these two variables. The exact data range used starts from 5 September 2008 (at 1206 LT) to 06 March 2014 (1005 LT). Figure 2 shows the outcome of C/NOFS vertical ion plasma drift and ΔH data with a correlation coefficient of 0.57 (number of data points is 3939) during local daytime (0700-1700 LT). Recently, *Kumar et al.* [2016] reported similar results by comparing EEJ and vertical $\mathbf{E} \times \mathbf{B}$ drifts from ROCSAT-1 in the Indian and Japanese sectors and over Jicamarca where a simultaneous comparison was done using JULIA and EEJ to assess the agreement at different altitudes. Using data during 2001-2013, *Kumar et al.* [2016] obtained correlation coefficient values of 0.61 and 0.56 betwen ROCSAT measurements and ΔH over the Indian and Japanese sectors, respectively. When separated according to levels of geomagnetic activity, correlation values during quiet conditions (Kp$<$ 3) were 0.6 and 0.52 over the Indian and Japanese sectors respectively during 2001-2003. It therefore appears that correlation values do not vary much based on geophysical conditions. Magnetometer data have temporal resolution of 1 minute and were used as a benchmark for choosing the co-

Table 1. RMSE and correlation coefficient (R) values between vertical $\mathbf{E} \times \mathbf{B}$ drift estimated from the C/NOFS vertical ion plasma drift-magnetometer ΔH relationship and available ISR measurements over Jicamarca during 2008-2014

Function of ΔH for $\mathbf{E} \times \mathbf{B}$ estimation	correlation coefficient (R)	RMSE (m/s)
Linear	0.762	7.27
Quadratic	0.774	7.309
Cubic	0.777	7.134
Fourth order polynomial	0.774	7.198
Fifth order polynomial	0.756	7.437

incidental C/NOFS data. A relationship between JULIA vertical $\mathbf{E} \times \mathbf{B}$ drifts and magnetometer ΔH has previously been established [*Anderson et al.*, 2004] over Jicamarca using 2001-2003 datasets. Among the different approaches investigated, *Anderson et al.* [2004] developed an expression estimating vertical $\mathbf{E} \times \mathbf{B}$ drifts as a third order polynomial function of ΔH using JULIA and magnetometer measurements during local daytime. We note that this expression was developed for datasets that were close in terms of altitude variations. Magnetometer ΔH is a proxy of EEJ which is the eastward current within the ionospheric E-region at $\simeq$ 120 km [*Richmond*, 1973; *Rastogi and Klobuchar*, 1990; *Anderson et al.*, 2004], while JULIA vertical $\mathbf{E} \times \mathbf{B}$ drift data are regarded as measurements at 150 km [e.g., *Kudeki and Fawcett*, 1993; *Chau and Woodman*, 2004; *Patra et al.*, 2014]. In our case, we are correlating ΔH (EEJ) at $\simeq$ 120 km with C/NOFS vertical ion plasma drift (altitude range of 400-550 km) and therefore should experimentally determine the appropriate mathematical function that best relates the two sets of measurements. To determine the solution, we tested a number of functions relating C/NOFS vertical ion plasma drift and ΔH (in Figure 2), and estimated vertical $\mathbf{E} \times \mathbf{B}$ drift for the entire ΔH database during times when the ISR made observations (over the period 2008-2014). The ISR observations were later used to validate the performance of each investigated expression. Table 1 shows the root mean square error, RMSE (m/s) and correlation coefficient (R) values for the different functions investigated.

In Table 1, statistical values indicate that vertical $\mathbf{E} \times \mathbf{B}$ is best estimated with a cubic function of ΔH which has the lowest RMSE (7.13 m/s) and high R (0.78) over the interval 2008-2014. We suggest that this method can be adopted for other longitude sectors (since satellite data are available) where there are magnetometer measurements hence increasing day-to-day vertical $\mathbf{E} \times \mathbf{B}$ drift coverage that has been previously limited to regions with radar instrumentation. However the coefficients of the cubic function should be re-determined for each longitude sector under consideration to take into account local time effects such as contributions to vertical $\mathbf{E} \times \mathbf{B}$ drifts arising from E-region migrating and non-migrating tides and longitudinal conductivity differences [*Millward et al.*, 2001; *Lühr et al.*, 2008]. A vital aspect to mention is that our study included the extended low solar activity period of 2008-2010 where low correlation between solar activity and vertical drift has been reported over the African sector [*Dubazane et al.*, 2018]. Observations during the extended solar minimum of 2008-2009 showed complex behaviour as they disagreed with the previously established understanding that vertical $\mathbf{E} \times \mathbf{B}$ drifts have solar activity dependance [e.g., *Richmond*, 1973; *Fejer et al.*, 1991] over the equatorial latitudes. Figure 3(a) shows the JULIA vertical $\mathbf{E} \times \mathbf{B}$ drift variability from 2001-2015 at 1200 LT. The solar flux F10.7 is superimposed on Figure 3(a) and generally shows little correlation from 2008-2010 which may be directly related to the complexity of the ionospheric variability during this extended solar minimum period [*Chen et al.*, 2011; *Solomon et al.*, 2013; *Ezquer et al.*, 2014; *Perna and Pezzopane*, 2016]. In Figure 3(b) ISR vertical $\mathbf{E} \times \mathbf{B}$ drift changes are shown at 1200 LT during 2008-2014. Figure 3 generally demonstrates that JULIA data are more extensive than ISR data during our period of study 2008-2014. Based on the data presented in Figure 3(a) showing no clear correlation between vertical $\mathbf{E} \times \mathbf{B}$ drift velocities and solar activity during the extended solar minimum, we have also investigated developing separate expressions for estimating vertical $\mathbf{E} \times \mathbf{B}$ drift in 2008-2010 and 2011-2014; and compared results with the combined datasets' outputs. The final expressions are

$$\mathrm{E} \times \mathrm{B} = -6 \times 10^{-6} \Delta H^3 - 0.0002 \Delta H^2 + 0.399 \Delta H - 1.872, \quad \text{for} \quad 2008 - 2014 \tag{1}$$

$$\mathrm{E} \times \mathrm{B} = -3 \times 10^{-5} \Delta H^3 + 0.002 \Delta H^2 + 0.484 \Delta H + 0.123, \quad \text{for} \quad 2008 - 2010 \tag{2}$$

$$\mathrm{E} \times \mathrm{B} = 7 \times 10^{-6} \Delta H^3 - 0.001 \Delta H^2 + 0.361 \Delta H - 3.488, \quad \text{for} \quad 2011 - 2014 \tag{3}$$

Equations (1)-(3) were developed from the C/NOFS vertical ion plasma drift and ground-based magnetometer derived ΔH presented in Figure 2. The next section presents validation results of the developed expressions.

4 Results and Discussion

Figure 4 shows scatter plots of observed (JULIA and ISR) vertical $\mathbf{E} \times \mathbf{B}$ drift and (a) ΔH, (b) C/NOFS vertical $\mathbf{E} \times \mathbf{B}$ drift, (c) derived $\mathbf{E} \times \mathbf{B}$ drift using equation (1), (d) derived $\mathbf{E} \times \mathbf{B}$ drift using equations (2) and (3). The JULIA mode of the Jicamarca ISR provides E-region (~ 150 km) vertical irregularity drift assumed to be almost equivalent to the background vertical $\mathbf{E} \times \mathbf{B}$ drift as shown in literature [e.g., *Chau and Woodman*, 2004]. The ISR provides drift profiles (200-800 km) and this study used the publically available averaged drifts in the range 225-600 km. We should add that restricting ISR altitudes within the C/NOFS altitude (400-550 km) data consideration did not significantly change results. In Figure 4(a), the correlation between ΔH and JULIA vertical $\mathbf{E} \times \mathbf{B}$ drift is higher (0.833) than the corresponding value for ISR vertical $\mathbf{E} \times \mathbf{B}$ drift (0.778). When ISR altitude averaging was limited to 400-550 km, the correlation coefficient value slightly changed to 0.75. The difference in correlation values between ΔH and JULIA/ISR vertical drifts is expected due to the altitudinal difference at which JULIA and ISR provide $\mathbf{E} \times \mathbf{B}$ measurements. While JULIA vertical $\mathbf{E} \times \mathbf{B}$ drift data (at lower bottomside F2 region of 150 km altitude) can be regarded as observations at constant altitude, it has been demonstrated that ISR vertical $\mathbf{E} \times \mathbf{B}$ drifts have temporal altitudinal variability exhibiting a general increase and decrease with altitude during morning and afternoon hours respectively [e.g., *Pingree and Fejer*, 1987; *Hui and Fejer*, 2015]. Correlation results in Figure 4(b) for the case of JULIA and C/NOFS vertical $\mathbf{E} \times \mathbf{B}$ give $R_{\text{JULIA}} = 0.72$ compared to $R_{\text{ISR}} = 0.53$ for ISR and C/NOFS vertical $\mathbf{E} \times \mathbf{B}$. Due to the altitude consideration, one would expect the correlation to be higher for C/NOFS and ISR vertical drifts. It is noted that there were less cases of coincidental C/NOFS and ISR vertical drifts observations, making it a bit difficult to conclude based on limited information. Relatively low correlation between C/NOFS vertical $\mathbf{E} \times \mathbf{B}$ drift and JULIA/ISR measurements (compared to R values for ΔH and ISR/JULIA data) is partly attributed to the different physical mechanisms at different altitudes, and the fact that a longitudinal range of 16° for C/NOFS vertical $\mathbf{E} \times \mathbf{B}$ drift is considered.

In terms of correlation with respect to local time dependance, Table 2 shows R values computed between ΔH and C/NOFS vertical ion plasma drift, and derived and observed ISR/JULIA $\mathbf{E} \times \mathbf{B}$ drift during 2008-2014 at different times with interval of 2 hours. While the R values between ΔH and C/NOFS vertical ion plasma drift are significantly lower for 13:00-15:00 LT and 15:00-17:00 LT, we see higher (above 0.7) R val-

Table 2. Correlation coefficient values for different local time ranges during 2008-2014 over Jicamarca

Local time range	Correlation coefficient (R) between		
	ΔH (nT) and C/NOFS vertical ion drift (m/s)	Derived and observed ISR $\mathbf{E} \times \mathbf{B}$ (m/s)	Derived and observed JULIA $\mathbf{E} \times \mathbf{B}$ (m/s)
07:00-09:00	0.558	0.802	0.820
09:00-11:00	0.583	0.705	0.868
11:00-13:00	0.524	0.766	0.847
13:00-15:00	0.385	0.833	0.818
15:00-17:00	0.230	0.803	0.737

ues between derived and observed ISR/JULA $\mathbf{E} \times \mathbf{B}$ drift at all local times. Starting from the developed expression relating ΔH and C/NOFS vertical ion plasma drift; which was later used to derive both ISR and JULIA vertical $\mathbf{E} \times \mathbf{B}$ drift at times when their observations were available, we notice that the primary trend determinant of the derived vertical $\mathbf{E} \times \mathbf{B}$ drift values is ΔH. Therefore if the trend behavior of vertical drift variability is captured in ΔH changes (which is usually the case), we expect improved results of derived ISR/JULIA vertical $\mathbf{E} \times \mathbf{B}$ drift. In this case, the coefficients will affect mainly the magnitude and not the trend of the derived values. The R values between ΔH and C/NOFS vertical ion plasma drift, derived and observed ISR vertical $\mathbf{E} \times \mathbf{B}$ drift; and derived and observed JULIA vertical $\mathbf{E} \times \mathbf{B}$ drift are 0.534, 0.766 and 0.846 respectively during 1000-1400 LT. The general high correlation between derived and observed JULIA vertical $\mathbf{E} \times \mathbf{B}$ drift could be due to the fact that the altitudinal difference between the EEJ (ΔH) and JULIA observations is relatively small (about 40 km) compared to the range of ISR or C/NOFS observations. Additionally, afternoon downward drifts observed in C/NOFS data have been reported [*Stoneback et al.*, 2011] which were found to be absent in JULIA 150 km echo drifts [*Rodrigues et al.*, 2015]. This is partly responsible for the lower R values reported in Table 2 during 13:00-17:00 LT as the downward drifts seen in C/NOFS vertical ion plasma drift could be absent in ΔH. Overall, during 1300-1500 LT and 1500-1700 LT, simultaneous occurrence of negative C/NOFS vertical ion plasma drift and ΔH accounted for 5.99% and 5.56% respectively. For the 1300-1500 LT range, negative values of C/NOFS vertical ion plasma drift made up 31% in comparison with 11% for ΔH. These values slightly changed to 36% and 10% for C/NOFS vertical ion plasma drift and ΔH respectively during 1500-1700 LT. Figure 4(b) was generated by limiting C/NOFS vertical $\mathbf{E}\times\mathbf{B}$ drift observations within ±4 degrees latitude and 77.2°W±8° geographic longitude around Jicamarca. Previous studies have used an extended latitude of about 8° − 10° away from the geomagnetic equator [e.g., *Patra et al.*, 2014; *Stoneback et al.*, 2011; *Yizengaw et al.*, 2014] and obtained high correlation values with 150 km echo radar measurements [e.g., *Patra et al.*, 2014]. However, for the development of the relationship involving EEJ derived data that is applicable over an extended period covering different solar activity levels, it is necessary to limit the latitude range to within the EEJ region in our analysis. Using the developed relationship in equation (1) (that comprised data in Figure 2 from 2008-2014) to derive vertical $\mathbf{E}\times\mathbf{B}$ drift during periods when the ISR and JULIA made measurements, the scatter plot between derived and observed values is shown in Figure 4(c). It is observed that there is a slight improvement in the correlation for ISR and JULIA observations with R values of 0.791 and 0.841 respectively when compared with ΔH (Figure 4(a)). Previously, *Anderson et al.* [2004] developed the same order of polynomial function of ΔH based on JULIA vertical $\mathbf{E}\times\mathbf{B}$ drift. Interestingly, a direct comparison (not shown) with *Anderson et al.* [2004] expression gives R values of 0.76 and 0.83 for ISR and JULIA vertical $\mathbf{E}\times\mathbf{B}$ drift respectively during 2008-2014. Considering expressions developed separately for low (2008-2010) and high (2011-2014) solar activity periods (using expressions in equations (2) and (3)) due to the extended nature of the deep solar minimum, the results are shown in Figure 4(d) for derived vertical drift denoted as $\mathbf{E}\times\mathbf{B_s}$ and observations from JULIA and ISR. The accuracy is almost the same and so the development of separate expressions seems not to significantly change results. This agrees with the study of *Rodrigues et al.* [2015] which found that the extreme solar minimum during 2008-2009 did not lead to noticeable changes/effects in daytime JULIA vertical $\mathbf{E}\times\mathbf{B}$ drifts. We however think that if F10.7 or any solar activity indicator was used as an input, the results would perhaps be different and so it is advantageous to use ΔH that seems to exhibit the inherent behaviour of $\mathbf{E}\times\mathbf{B}$ changes. From now onwards, the discussion will only use derived vertical $\mathbf{E}\times\mathbf{B}$ drifts using equation (1) that contains coefficients from the entire dataset (2008-2014) used in our study.

Figure 5 shows the distribution of the differences (observed-derived) between the derived and observed vertical $\mathbf{E}\times\mathbf{B}$ drift velocities for (a) ISR and (b) JULIA in 2008-2004. In both cases, the mean differences are close to 0 m/s and the standard deviation values are basically the same. For both ISR and JULIA vertical $\mathbf{E}\times\mathbf{B}$ observations, at

Table 3. Summary of correlation coefficient and RMSE values for different storm periods with Dst≤-100 nT during 2008-2016 when ΔH and vertical drift data were simultaneously available over Jicamarca

Storm period	Minimum Dst (nT)	R	RMSE (m/s)	Data source
05-08 August 2011	-107	0.92	4.37	ISR
08-11 March 2012	-131	0.87	4.31	JULIA
08-10 October 2012	-105	0.77	7.06	JULIA (only 08th had data)
13-15 November 2012	-108	0.96	3.88	JULIA (only 14th had data)
25-27 August 2015	-100	0.78	5.08	ISR
07-08 October 2015	-124	0.80	5.99	JULIA
19-21 January 2016	-104	0.92	4.99	JULIA (19th and 20th had data)

least 80% of differences lie within -5 m/s and 5 m/s when the developed relationship is validated over the entire available respective datasets during 2008-2014. We have investigated the potential of the developed expression in estimating local daytime vertical $\mathbf{E} \times \mathbf{B}$ response during geomagnetic storms. For this purpose, we considered strong geomagnetic storms with Dst≤-100 nT during 2008-2016 when ISR and JULIA observations were simultaneously available with ΔH measurements. Table 3 shows the summary of correlation coefficient and RMSE values for different storm periods with Dst≤-100 nT during 2008-2016 when we had ΔH and vertical drift data over Jicamarca. There were only two storm periods when ISR vertical drifts and ΔH were present. Important to point out is that Table 3 contains results of 2015 and 2016 which were not covered during the process of developing the expression relating C/NOFS ion drifts and ΔH. Given that correlation coefficient values are above 0.75 in all cases with RMSE values comparable to some previous studies [e.g., *Anderson et al.*, 2004] and even lower in some cases as is the case for the 13-15 November 2012 storm period (despite the limited dataset available), we suggest that the developed relation can be utilized for all geophysical conditions. We re-state that *Anderson et al.* [2004] obtained a RMSE value of 3.79 m/s using the same order of polynomial on ΔH and JULIA vertical drifts data during 2001-2003.

In details, we present results for storm periods of 05-08 August 2011 and 08-10 March 2012 when ISR and JULIA observations were available respectively. In both cases, we have compared our expression's performance with the earlier developed expression by

Anderson et al. [2004]. Figure 6 shows the observed (black dots) and derived $\mathbf{E}\times\mathbf{B}$ drift during the storm period of 05-08 August 2011. The derived vertical $\mathbf{E}\times\mathbf{B}$ drift velocities based on C/NOFS vertical $\mathbf{E}\times\mathbf{B}$ and ΔH expression are plotted as red dots. Corresponding values based on JULIA vertical $\mathbf{E}\times\mathbf{B}$ and ΔH relationship (expressed as $(\mathbf{E}\times\mathbf{B})_{\mathbf{A2004}}$) from *Anderson et al.* [2004] are shown in blue dots. In the subsequent graphical representation where diurnal vertical $\mathbf{E}\times\mathbf{B}$ drift comparisons are performed, the colors of respective observed and derived vertical $\mathbf{E}\times\mathbf{B}$ drifts are similar to the description above. Shown in Figure 6(a) are the symmetric disturbance field in the H-component, SYM-H (nT) and Bz component of the interplanetary magnetic field, IMF Bz (nT) in red and blue curves respectively. The SYM-H index is equivalent to high resolution Dst index [*Wanliss and Showalter*, 2006] and provides information about storm-time ring current system. The occurrence of the 05 August 2011 geomagnetic storm was a result of complex changes in solar wind conditions that involved the launching of three coronal mass ejections on 02-03 August and became geoeffective on 04-05 August 2011 [*Huang et al.*, 2014]. On the 06 August 2011 at 0322 UT, the SYM-H reached its peak value (-132 nT) of the main-phase and thereafter the recovery process started and lasted at least 3 days. Figure 6 shows that at the commencement of the main phase onset (1906 UT or 1357 LT over Jicamarca on 05 August 2011), there was a sharp increase in vertical $\mathbf{E}\times\mathbf{B}$ drift (Figure 6(b) on 05 August 2011) which is a manifestation of penetrating electric field of magnetospheric origin [e.g., *Fejer and Scherliess*, 1995, 1998; *Huang et al.*, 2005] during the southward turning of IMF Bz and this was well reproduced by the developed mathematical expression (red dots). On the 06 August 2011 during the recovery phase, the local daytime vertical drift decreased probably due to the westward electric field generated by the disturbed ionospheric dynamo [e.g., *Blanc and Richmond*, 1980; *Huang*, 2013] and the dominance of R2 current when IMF Bz turns north [e.g., *Kikuchi et al.*, 2000; *Yizengaw et al.*, 2011]. The developed expression not only follows the decreased vertical $\mathbf{E}\times\mathbf{B}$ velocities, but also estimates well the magnitude of the vertical drifts. Overall, we obtained a high R value (0.92) between observed and derived vertical $\mathbf{E}\times\mathbf{B}$ drift velocities during the storm period of 05-08 August 2011. The computed RMSE of 4.37 m/s is less than the corresponding result (RMSE=6.77 m/s) generated for the same order of polynomial in *Anderson et al.* [2004] which estimated vertical $\mathbf{E}\times\mathbf{B}$ velocities based on JULIA and ΔH measurements. The R value is similar (0.92) for both approaches during this storm period. What is significant is that our approach uses C/NOFS vertical $\mathbf{E}\times\mathbf{B}$ drift and ΔH observations and may be applicable even during geomagnetic storm conditions as shown in Figure 6(b). Despite the differences in accuracy, the earlier developed relationship [*Anderson et al.*, 2004] also follows the vertical $\mathbf{E} \times \mathbf{B}$ drift variability during this storm period. Figure 7 shows a comparison of JULIA observed and derived vertical $\mathbf{E} \times \mathbf{B}$ drift velocities for geomagnetically disturbed period of 08-10 March 2012. Figure 7(a) presents variations of SYM-H (nT) and IMF Bz (nT) plotted in red and blue colors respectively. The vertical black dashed lines correspond to the times of the shock (1103 UT) and storm main phase onset (0100 UT) on 08 March and 09 March 2011 respectively. The solar wind conditions and interplanetary causes of this storm period are detailed in *Tsurutani et al.* [2014]. While the shock hit the Earth's magnetosphere at 1103 UT on 08 March, the storm main phase occured on 09 March 2012 with SYM-H (nT) index reaching -148 nT at around 0800 UT. In Figure 7(b), the observed (black dots) and derived (red and blue dots) vertical $\mathbf{E} \times \mathbf{B}$ drift velocities are compared during local daytime. Unfortunately there were no JULIA vertical $\mathbf{E} \times \mathbf{B}$ drift observations as well as ΔH to derive $\mathbf{E} \times \mathbf{B}$ velocities on 08 March 2012. For the rest of the storm period, the variations in JULIA vertical $\mathbf{E} \times \mathbf{B}$ velocities are captured by the corresponding derived $\mathbf{E} \times \mathbf{B}$ drift velocities (red dots) with some occasional overestimation as is the case at around 1552 UT on 09 March during the sharp increase of the vertical $\mathbf{E} \times \mathbf{B}$ drift believed to be due to penetrating electric fields [*Habarulema et al.*, 2016]. Nevertheless, the derived vertical $\mathbf{E} \times \mathbf{B}$ drifts respond to the most important physical feature where penetrating electric fields of magnetospheric origin enhances the daytime eastward electric field in equatorial latitudes. For our approach based on C/NOFS vertical $\mathbf{E} \times \mathbf{B}$ and ΔH, the computed R and RMSE values are 0.87 and 4.31 m/s respectively during the 09-11 March 2012. The approach in *Anderson et al.* [2004] gives R and RMSE values of 0.90 and 6.67 m/s respectively; and generally underestimates the observed vertical $\mathbf{E} \times \mathbf{B}$ drift velocities (see blue dots in Figure 7(b)). Generally, based on results in Figures 6-7 and Table 3, it is feasible to conclude that the developed expression based on C/NOFS vertical $\mathbf{E} \times \mathbf{B}$ drift and magnetometer ΔH observations is applicable in estimating vertical $\mathbf{E} \times \mathbf{B}$ velocities during geomagnetic storm conditions. Mathematically, this is possible and understandable as most of the daytime time vertical drift changes are reflected in the EEJ (ΔH) measurements which respond identically to vertical $\mathbf{E} \times \mathbf{B}$ drift during magnetically disturbed conditions.

Finally, we validate our expression during other periods not covered by the data which was used to develop it. We recall that equation (1) was developed using C/NOFS

Table 4. Correlation coefficient (R) and root mean square error (RMSE) values computed using observed (ISR and JULIA) and derived vertical $\mathbf{E}\times\mathbf{B}$ (m/s) for some days in 2014. Observed ISR and JULIA vertical $\mathbf{E}\times\mathbf{B}$ (m/s) are compared with corresponding vertical $\mathbf{E}\times\mathbf{B}$ (m/s) obtained using our expression based on C/NOFS vertical $\mathbf{E}\times\mathbf{B}$ (denoted as C/NOFS(ΔH) func) and *Anderson et al.* [2004] relationship (denoted as JULIA(ΔH) func) respectively.

ISR with:	C/NOFS(ΔH) func		JULIA(ΔH) func		JULIA with:	C/NOFS(ΔH) func		JULIA(ΔH) func	
Date (2014)	R	RMSE (m/s)	R	RMSE (m/s)	Date (2014)	R	RMSE (m/s)	R	RMSE (m/s)
23 April	0.83	2.77	0.83	4.38	27 June	0.95	2.81	0.95	5.30
06 May	0.88	5.06	0.86	5.81	28 July	0.95	3.84	0.95	3.70
26 Nov	0.89	7.20	0.89	2.42	28 Aug	0.83	9.01	0.88	3.61
16 Dec	0.79	6.37	0.78	3.28	08 Dec	0.97	4.88	0.97	4.05

vertical ion plasma drift (equivalent to $\mathbf{E}\times\mathbf{B}$) velocities and ΔH during the period of September 2008 to March 2014. Figure 8 shows observed and derived vertical $\mathbf{E}\times\mathbf{B}$ velocities on randomly chosen days within the period of May-December 2014 when ISR and JULIA made observations. Our approach is once again compared with derived vertical $\mathbf{E}\times\mathbf{B}$ drift velocities generated using expression in *Anderson et al.* [2004], which was developed based on JULIA and ΔH observations. Figure 8(a) graphically compares observed ISR (black dots) and derived (red and blue dots for our relationship and *Anderson et al.* [2004] expression respectively) vertical $\mathbf{E}\times\mathbf{B}$ velocities for 23 April 2014, 06 May 2014, 26 November 2014 and 16 December 2014 during local daytime (0700-1700 UT). Figure 8(b) is similar to Figure 8(a), but for JULIA and derived vertical $\mathbf{E}\times\mathbf{B}$ velocities on days 27 June 2014, 28 July 2014, 28 August 2014 and 08 October 2014. The statistical summary for the comparisons is presented in Table 4. In all cases, the R values computed from observed and our derived vertical $\mathbf{E}\times\mathbf{B}$ drift velocities are highly similar/comparable to the corresponding results when *Anderson et al.* [2004] expression is used. In terms of RMSE, with exception of 27 June 2014, the *Anderson et al.* [2004] expression gives lower values for observed JULIA vertical $\mathbf{E}\times\mathbf{B}$ drift comparisons. This is an expected result as *Anderson et al.* [2004] developed their expression based on JULIA vertical $\mathbf{E}\times\mathbf{B}$ drift and ΔH observations.

Figure 8 and Table 4 essentially demonstrate that it is possible to follow diurnal changes in vertical $\mathbf{E} \times \mathbf{B}$ drift velocities based on the polynomial function developed using C/NOFS vertical ion plasma drift and ΔH observations. This opens up new opportunities to develop low latitude vertical $\mathbf{E} \times \mathbf{B}$ drift models using a combination of satellite and magnetometer measurements especially during local daytime that is accurate in all longitude sectors. In fact such models can be valid for all local times since satellites would also provide observations during nighttime (although sparse). Magnetometer measurements which are continuous and have high temporal resolution would then provide reliable day-time vertical $\mathbf{E} \times \mathbf{B}$ drift database. Pairs of magnetometers that satisfy the requirements to allow the development of expressions (similar to what has been done in this study) in different longitude sectors exist [e.g., *Yizengaw et al.*, 2011, 2014] in African, American, Indian and Asian sectors. Therefore, based on the presented results and approach, it is possible to develop new empirical vertical $\mathbf{E} \times \mathbf{B}$ drift models and update the existing ones such as the Scherliess-Fejer (SF) model [*Scherliess and Fejer*, 1999] and the ROCSAT-1 based quiet equatorial model [*Fejer et al.*, 2008] to account for the recent unusual changes in solar activity such as the extended solar minimum of 2008-2010.

5 Conclusions

For the first time, a mathematical relationship between C/NOFS vertical ion plasma drift (equivalent to $\mathbf{E} \times \mathbf{B}$ drift at about 400 km) and magnetometer ΔH observations has been developed and validated with ISR and JULIA observations during local daytime (0700-1700 UT) covering a period of 2008-2014. While we restricted our analysis to Jicamarca (11.8°S, 77.2°W; 0.8°N geomagnetic) due to the availability of the actual observations to validate our approach, the order of the developed function is transferable to different longitude sectors which have magnetometer locations that can estimate the EEJ. We stress that while the order of the polynomial can be kept, new coefficients should be derived for a different longitude sector to account for local contributions to vertical $\mathbf{E} \times \mathbf{B}$ velocities such as E region tides (both migrating and nonmigrating) influence on the electric field [*Millward et al.*, 2001; *Lühr et al.*, 2008; *Maute et al.*, 2012]. Overall, the developed expression can reconstruct at least 75% of the observed vertical $\mathbf{E} \times \mathbf{B}$ drift velocities from the ISR and JULIA observations. Of significant importance is the robustness of the polynomial function to also estimate vertical $\mathbf{E} \times \mathbf{B}$ drift velocities during geomagnetic storms. Given the recent developments in magnetometer deployments to estimate the EEJ in different longitude sectors [*Yizengaw et al.*, 2014], we suggest that the developed approach is a suitable basis for developing high resolution empirical vertical $\mathbf{E}\times\mathbf{B}$ models even in longitudes without radar observations.

Acknowledgments

C/NOFS vertical $\mathbf{E}\times\mathbf{B}$ drift data was obtained from http://spdf.gsfc.nasa.gov/pub/data/cnofs/cindi/. The C/NOFS mission is supported by the Air Force Research Laboratory, the Department of Defense Space Test Program, the National Aeronautics and Space Administration (NASA), the Naval Research Laboratory, and the Aerospace Corporation. ISR and JULIA data were obtained from jro.igp.gob.pe. IMF Bz data are available from the Space Physics Data Facility website omniweb.gsfc.nasa.gov. The SYM-H index data was accessed from the World Data Centre, Kyoto, Japan http://wdc.kugi.kyoto-u.ac.jp. This work is based on the research supported in part by the National Research Foundation of South Africa (Grant Number 105778) and opinions, findings and conclusions or recommendations expressed in this paper are of the author(s), and the NRF accepts no liability whatsoever in this regard. EY's work has been partially supported by AFOSR (FA9550-12-1-0437 and FA9550-15-1-0399) and NSF AGS145136 grants. MBM was partially supported by the NSF grants AGS-1450512 and AGS-1654044.

References

Anderson, D., A. Anghel, K. Yumoto, M. Ishitsuka, and E. Kudeki, Estimating daytime vertical E×B drift velocities in the equatorial F-region using ground-based magnetometer observations, *Geophys. Res. Lett*, *29*(12), 1596, doi:10.1029/2001GL014562, 2002.

Anderson, D., A. Anghel, J. Chau, and O. Veliz (2004), Daytime vertical E× B drift velocities inferred from ground-based magnetometer observations at low latitudes, *Space Weather*, *2*(S11001), doi:10.1029/2004SW000095.

Blanc, M., and A. D. Richmond, The ionospheric disturbance dynamo, *J. Geophys. Res.*, *85*, 1669–1686, 1980.

Chau, J. L., and R. F. Woodman, Daytime vertical and zonal velocities from 150-km echoes: Their relevance to F-region dynamics, *Geophys. Res. Lett.*, *31*, doi:10.1029/2004GL020800, 2004.

Chen, Y., L. Liu and W. Wan (2011), Does the F10.7 index correctly describe solar EUV flux during the deep solar minimum of 2007-2009?, *Journal of Geophysical Research*, *116*(A04304), doi:10.1029/2010JA016301.

Dubazane, M. B, J. B. Habarulema, and J. C. Uwamahoro (2018), Modelling ionospheric vertical drifts over Africa low latitudes using Empirical Orthogonal functions and comparison with climatological model, *Adv. Space Res.*, *61*, 326–336, https://doi.org/10.1016/j.asr.2017.10.024.

Ezquer, R. G., J. L. López, L. A. Scidá, M. A. Cabrera, B. Zolesi, C. Bianchi, M. Pezzopane, E. Zuccheretti, and M. Mosert (2014), Behaviour of ionospheric magnitudes of F2 region over Tucumán during a deep solar minimum and comparison with the IRI 2012 model predictions, *Journal of Atmospheric and Solar-Terrestrial Physics*, *107*, 89–98, doi:http://dx.doi.org/10.1016/j.jastp.2013.11.010.

Fejer, B. G., E. R. de Paula, S. A. Gonzalez and R. F. Woodman, Average vertical and zonal F region plasma drifts over Jicamarca, *J. Geophys. Res. Space Physics*, *96*(A8), 13901–13906, 1991.

Fejer, B. G., J. W. Jensen, and S. -Y. Su, Quiet time equatorial F region vertical plasma drift model derived from ROCSAT-1 observations, *J. Geophys. Res. Space Physics*, *113*(A05304), doi:10.1029/2007JA012801.

Fejer, B. G., and L. Scherliess, Time dependent response of equatorial ionospheric electric field to magnetospheric disturbances, *Geophys. Res. Lett.*, *22*(7), 851–854, 1995.

Fejer, B. G., and L. Scherliess, Mid- and low-latitude prompt ionospheric zonal plasma drifts, *Geophys. Res. Lett.*, *25*(16), 3071–3074, 1998.

Habarulema, J. B., Z. T. Katamzi, E. Yizengaw, Y. Yamazaki and G. Seemala, Simultaneous storm time equatorward and poleward large-scale TIDs on a global scale, *Geophys. Res. Lett.*, (43), 6678–6686, 2016.

Huang, C. M., A. D. Richmond, and M. -Q. Chen, Theoretical effects of geomagnetic activity on low-latitude electric fields, *J. Geophys. Res.*, *110*, A05312, doi: 10.1029/2004JA010994, 2005.

Huang, C. M., Disturbance dynamo electric fields in response to geomagnetic storms occuring at different universal times, *J. Geophys. Res.*, *118*, 496–501, 2013.

Huang, C. Y., Y. -J. Su, E. K. Sutton, D. R. Weimer and R. L. Davidson, Energy coupling during the August 2011 magnetic storm, *J. Geophys. Res.*, *119*, 1219–1232, doi: 10.1002/2013JA01297, 2014.

Hui, D., and B. G. Fejer, Daytime plasma drifts in the equatorial lower ionosphere, *J. Geophys. Res. Space Physics*, *120*, 9738–9747, doi:doi:10.1002/2015JA021838, 2015.

Huber, P. J (1981), Robust Statistics, *John Wiley & Sons*, New York, USA.

Huber, P. J, and E. M. Ronchetti (2009), Robust Statistics: Second Edition, *John Wiley & Sons*, New York, USA.

Kikuchi, T., H. Lühr, K. Schlegel, H. Tachihara, M. Shinohara and T. -I. Kitamura (2000), Penetration of auroral electric fields to the equator during a substorm, *J. Geophys. Res.*, *105*(A10), 23251–23261.

Kumar, S., B. Veenadhari, S. Tulasi Ram, S.-Y. Su, and T. Kikuchi (2016), Possible relationship between the equatorial electrojet (EEJ) and daytime vertical E×B drift velocities in F region from ROCSAT observations, *Advances in Space Research*, *58*, 1168–1176, http://dx.doi.org/10.1016/j.asr.2016.06.009.

Kudeki, E., and C. D. Fawcett (1993), High resolution observations of 150 km echoes at Jicamarca, *Geophys. Res. Lett.*, *20*, 1987–1990, doi:10.1029/93GL01256.

Leys, C., C. Ley, O. Klein, P. Bernard, and L. Licata (2013), Detecting outliers: Do not use standard deviation around the mean, use absolute deviation around the median, *Journal of Experimental Social Psychology*, *49*(4), 764–766.

Lomidze, L., D. J. Knudsen, J. Burchill, A. Kouznetsov, and S. C. Buchert (2018), Calibration and Validation of Swarm Plasma Densities and Electron Temperatures Using Ground-Based Radars and Satellite Radio-Occultation Measurements, *Radio Science*, *53*, 15–36, doi: 10.1002/2017RS006415.

Lühr, H., M. Rother, K. Häusler, P. Alken and S. Maus (2008), The influence of nonmigrating tides on the longitudinal variation of the equatorial electrojet, *J. Geophys. Res. Space Physics*, *113*(A08313), doi:10.1029/2008JA013064.

Manoj, C., H. Lühr, S. Maus, and N. Nagarajan (2006), Evidence for short spatial correlation lengths of the noontime equatorial electrojet inferred from a comparison of satellite and ground magnetic data, *Journal of Geophysical Research: Space Physics*, *111*(A11), doi:10.1029/2006JA011855.

Maute, A., A. D. Richmond and R. G. Roble (2012), Sources of low-latitude ionospheric $\mathbf{E} \times \mathbf{B}$ drifts and their variability, *J. Geophys. Res. Space Physics*, *117*(A06312), doi: 10.1029/2011JA017502.

Millward, G. H., I. C. Müller-Wodarg, A. D. Aylward, T. J. Fuller-Rowell, A. D. Richmond and R. J. Moffett (2001), An investigation into the influence of tidal forcing on F region equatorial vertical ion drift using a global ionosphere-thermosphere model with coupled electrodynamics , *J. Geophys. Res. Space Physics*, *106*(A11), 24733–24744.

Patra, A. K., T. Yokoyama, Y. Otsuka, and M. Yamamoto (2008), Daytime 150 km echoes observed with the Equatorial Atmosphere Radar in Indonesia: First results, *Geophys. Res. Lett.*, *119*(5), 3777–3788, doi:10.1029/2007GL033130.

Patra, A. K., and N. V. Rao (2006), Radar observations of daytime 150 km echoes from outside the equatorial electrojet belt over Gadanki, *Geophys. Res. Lett.*, *33*(L03104), 1987–1990, doi:10.1029/2005GL024564.

Patra, A. K., P. P. Chaitanya, N. Mizutani, Y. Otsuka, T. Yokoyama, and M. Yamamoto (2012), A comparative study of equatorial daytime vertical $\mathbf{E}\times\mathbf{B}$ drift in the Indian and Indonesian sectors based on 150 km echoes, *J. Geophys. Res. Space Physics*, *117*(A11312), doi:10.1029/2012JA018053.

Patra, A., S. Sripathi, and D. Tiwari (2004), Coupling effect of the equatorial F region irregularities on the low latitude E region instability processes, *Geophysical Research Letters*, *31*(L17803), doi:10.1029/2004GL020486.

Patra, A. K., P. P. Chaitanya, Y. Otsuka, T. Yokoyama, M. Yamamoto, R. A. Stoneback, and R. A. Heelis (2014), Vertical $\mathbf{E}\times\mathbf{B}$ drifts from radar and C/NOFS observations in the Indian and Indonesian sectors: Consistency of observations and model, *J. Geophys. Res. Space Physics*, *119*(5), 3777–3788, doi:10.1002/2013JA019732.

Perna, L., and M. Pezzopane (2016), foF2 vs solar indices for the Rome station: Looking for the best general relation which is able to describe the anomalous minimum between cycles 23 and 24, *Journal of Atmospheric and Solar-Terrestrial Physics*, *148*, 13–21, http://dx.doi.org/10.1016/j.jastp.2016.08.003.

Pingree, J. E., and B. G. Fejer, On the height variation of the equatorial F region vertical plasma drifts, *J. Geophys. Res.*, *92 (A5)*, 4763–4766, 1987.

Rabiu, A. B., O. O. Folarin, T. Uozumi, N. S. A. Hamid and A. Yoshikawa (2017), Longitudinal variation of equatorial electrojet and the occurrence of its counter electrojet, *Annales Geophysicae*, *35*, 535–545, doi:doi:10.5194/angeo-35-535-2017.

Raghavarao, R., and B. G. Anandarao (1980), Vertical winds as a plausible cause for equatorial counter electrojet, *Geophys. Res. Lett*, *7* (5), 357–360, 1980.

Rastogi, R. G. (1974), Westward equatorial electrojet during daytime hours, *Journal of Geophysical Research*, *79*(10), 1503–1512.

Rastogi, R. G., and J. A. Klobuchar (1990), Ionospheric electron content within the equatorial F2 layer anomaly belt, *J. Geophys. Res.*, *95* (A11), 19045–19052, 1990.

Richmond, A. (1973), Equatorial electrojet—I. Development of a model including winds and instabilities, *Journal of Atmospheric and Terrestrial Physics*, *35*(6), 1083–1103, doi: 10.1016/0021-9169(73)90007-X.

Rousseeuw, P. J, and C. Croux (1993), Alternatives to the median absolute deviation, *Journal of the American Statistical Association*, *88*(424), 1273–1283.

Rodrigues, F. S., J. M. Smith, M. Milla, and R. A. Stoneback (2015), Daytime ionospheric equatorial vertical drifts during the 2008-2009 extreme solar minimum, *J. Geophys. Res. Space Physics*, *120*, 1452–1459, doi:10.1002/2014JA020478.

Scherliess, L., and B. G. Fejer (1997), Storm time dependence of equatorial disturbance dynamo zonal electric fields, *J. Geophys. Res. Space Physics*, *102*(A11), 24,037–24,046, doi:10.1029/97JA02165.

Scherliess, L., and B. G. Fejer (1999), Radar and satellite global equatorial F region vertical drift model, *J. Geophys. Res. Space Physics*, *104*(A4), 6829–6842, doi: 10.1029/1999JA900025.

Solomon, S., L. Qian, and A. G. Burns (2013), The anomalous ionosphere between solar cycles 23 and 24, *J. Geophys. Res. Space Physics*, *118*, 6524–6535, doi: 10.1002/jgra.50561.

Stoneback, R., R. Heelis, A. Burrell, W. Coley, B. G. Fejer, and E. Pacheco (2011), Observations of quiet time vertical ion drift in the equatorial ionosphere during the solar minimum period of 2009, *J. Geophys. Res. Space Physics*, *116*(A12327), doi: 10.1029/2011JA016712.

Stoneback, R. A., R. L. Davidson, and R. L. Heelis (2012), Ion drift meter calibration and photoemission correction for the C/NOFS satellite, *J. Geophys. Res. Space Physics*, *117*(A08323), doi:10.1029/2012JA017636.

Tsurutani, B. T., E. Echer, K. Shibata, O. P. Verkhoglyadova, A. J. Mannucci, W. D. Gonzalez, J. U. Kozyra, and M. Patzold, The interplanetary causes of geomagnetic activity during the 7âĂŞ17 March 2012 interval: a CAWSES II overview, *J. Space Weather Space Clim.*, *4*(A02), A02p1–A02p7, doi:10.1051/swsc/2013056, 2014.

Vineeth, C., T. K. Pant, and R. Sridharan (2009), Equatorial counter electrojets and polar stratospheric sudden warmings - a classical example of high latitude - low latitude coupling?, *Ann. Geophys.*, *27*, 3147–3153.

Wanliss, J. A., and K. M. Showalter (2006), High-resolution global storm index: *Dst* versus SYM-H, *J. Geophys. Res.*, *111*(A02202), doi:10.1029/2005JA011034.

Yizengaw, E., and M. B. Moldwin (2009), African Meridian B-field Education and Research (AMBER) Array, *Earth, Moon, and Planets*, doi:10.1007/s11038-008-9287-2.

Yizengaw, E., M. B. Moldwin, E. Zesta, C. M. Biouele, B. Damtie, A. Mebrahtu, B. Rabiu, C. E. Valladares, and R. Stoneback, The longitudinal variability of equatorial electrojet and vertical drift velocity in the African and American sectors, *Ann. Geophys.*, *32*, 231–238, 2014.

Yizengaw, E., M. B. Moldwin, A. Mebrahtu, B. Damtie, E. Zesta, C. E.Valladares, and P. H. Doherty, Comparison of storm time equatorial ionospheric electrodynamics in the African and American sectors, *J. Atmos. Solar-Terr. Phys.*, *73*(1), 156–163, 2011.

Yizengaw, E., E. Zesta, M. B. Moldwin, B. Damtie, A. Mebrahtu, C. E. Valladares, and R. F. Pfaff, Longitudinal differences of ionospheric vertical density distribution and equatorial electrodynamics , *J. Geophys. Res. Space Phys.*, *A07312*, doi:10.1029/2011JA017,454, 2012.

figures and captions.

Figure file for "2017JA025144"

Habarulema J. B., Dubazane M. B., Katamzi-Joseph Z. T., Yizengaw E., Moldwin M. B. and Uwamahoro J. C.

May 21, 2018

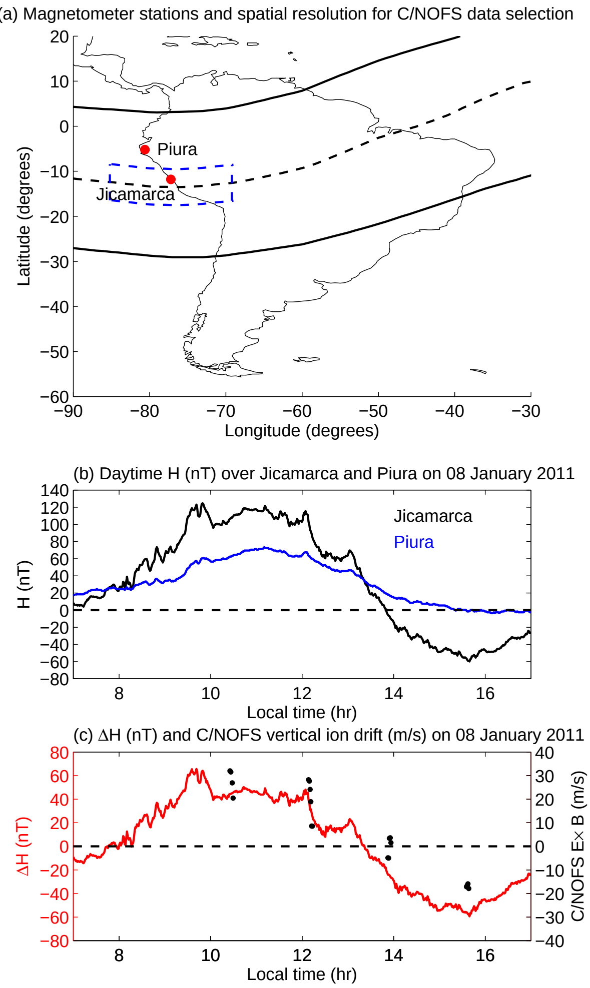

Figure 1: (a) Location of magnetometer stations (red dots), illustration of the spatial coverage (within the blue enclosure) used for C/NOFS vertical ion drift data consideration within altitude of 400-550 km around Jicamarca, (b) daytime H (nT) after removing the background H value by subtracting the average nighttime baseline value between 2300-0300 local time over Jicamarca (black curve) and Piura (blue curve) for 08 January 2011, and (c) daytime ΔH (nT) or simply EEJ obtained using data in (b) along with available C/NOFS vertical ion drift (m/s) (plotted as black dots) on 08 January 2011. In (a), the dashed black line represents the geomagnetic equator while the solid black lines show the southern and northern crests of the equatorial ionisation anomaly at ±15° from the geomagnetic equator.

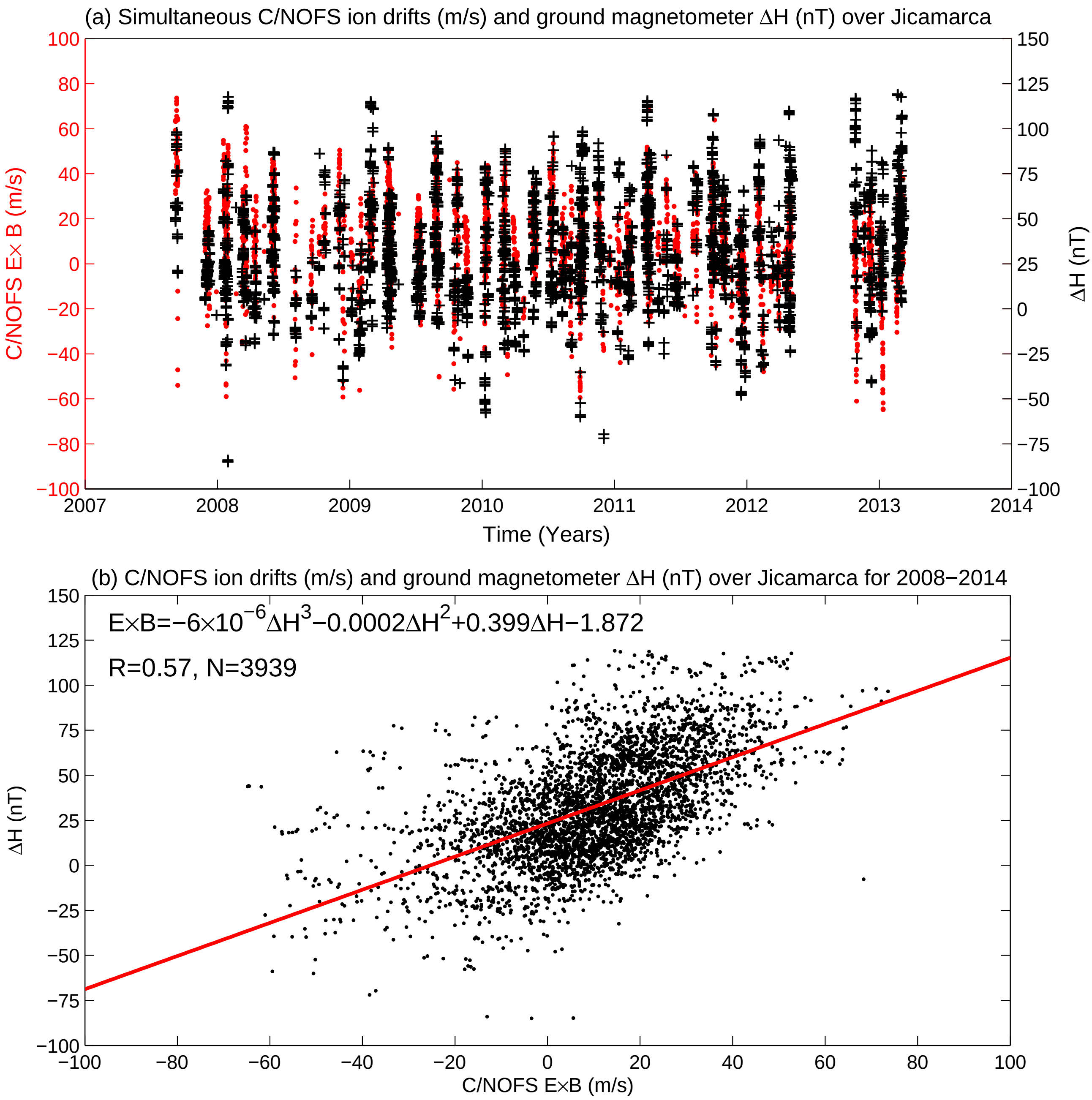

Figure 2: Representation of (a) simultaneous C/NOFS vertical ion plasma drifts (**red dots**) equivalent to vertical $\mathbf{E} \times \mathbf{B}$ drift (m/s) and ΔH (nT) (black positive sign) availability (2008-2014) over Jicamarca during local daytime (0700-1700 LT); and (b) **scatter plot of C/NOFS vertical ion plasma drift or $\mathbf{E} \times \mathbf{B}$ drift (m/s) and ΔH (nT). The derived cubic expression is shown in (b) along with correlation coefficient (R)** of 0.57 obtained using 3939 number of observations.

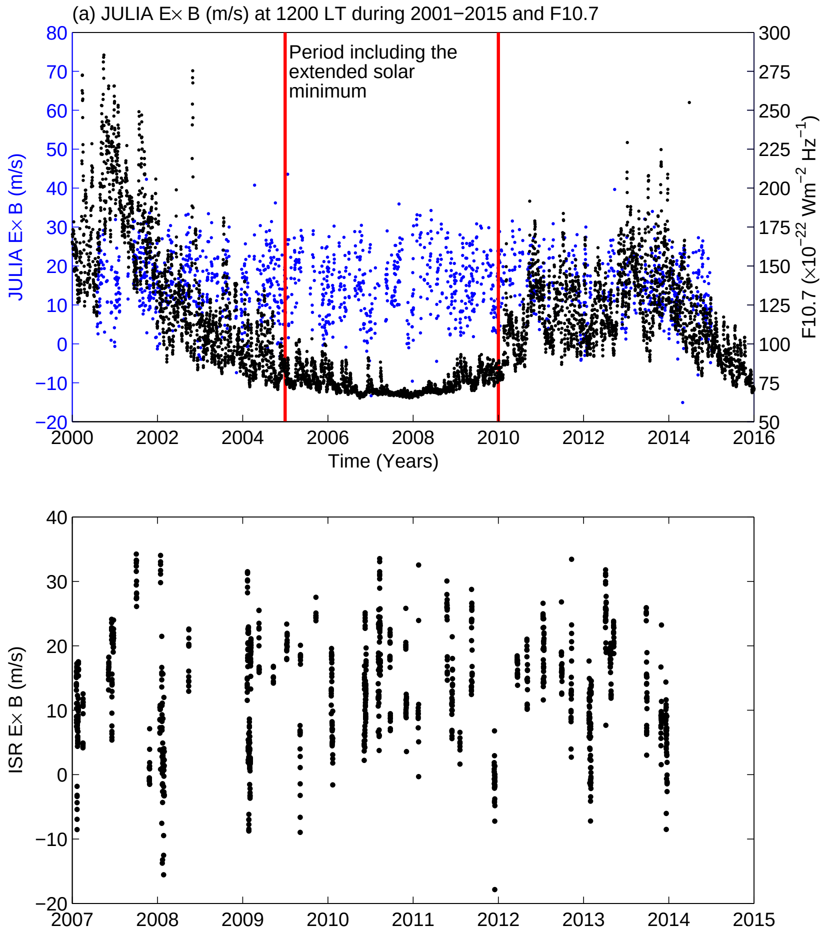

Figure 3: (a) Comparison of JULIA vertical $\mathbf{E} \times \mathbf{B}$ (m/s) variability at 1200 LT (2001-2015) with solar flux at 10.7 cm wavelength, F10.7 (2000-2016). The vertical red lines highlight the period (2005-2010) including the prolonged solar minimum. **Panel (b) shows an example of ISR E × B (m/s) availability at 1200 LT from 2008-2014 used in evaluating the derived expression between C/NOFS vertical ion drifts and ground-based magnetometer ΔH (nT).**

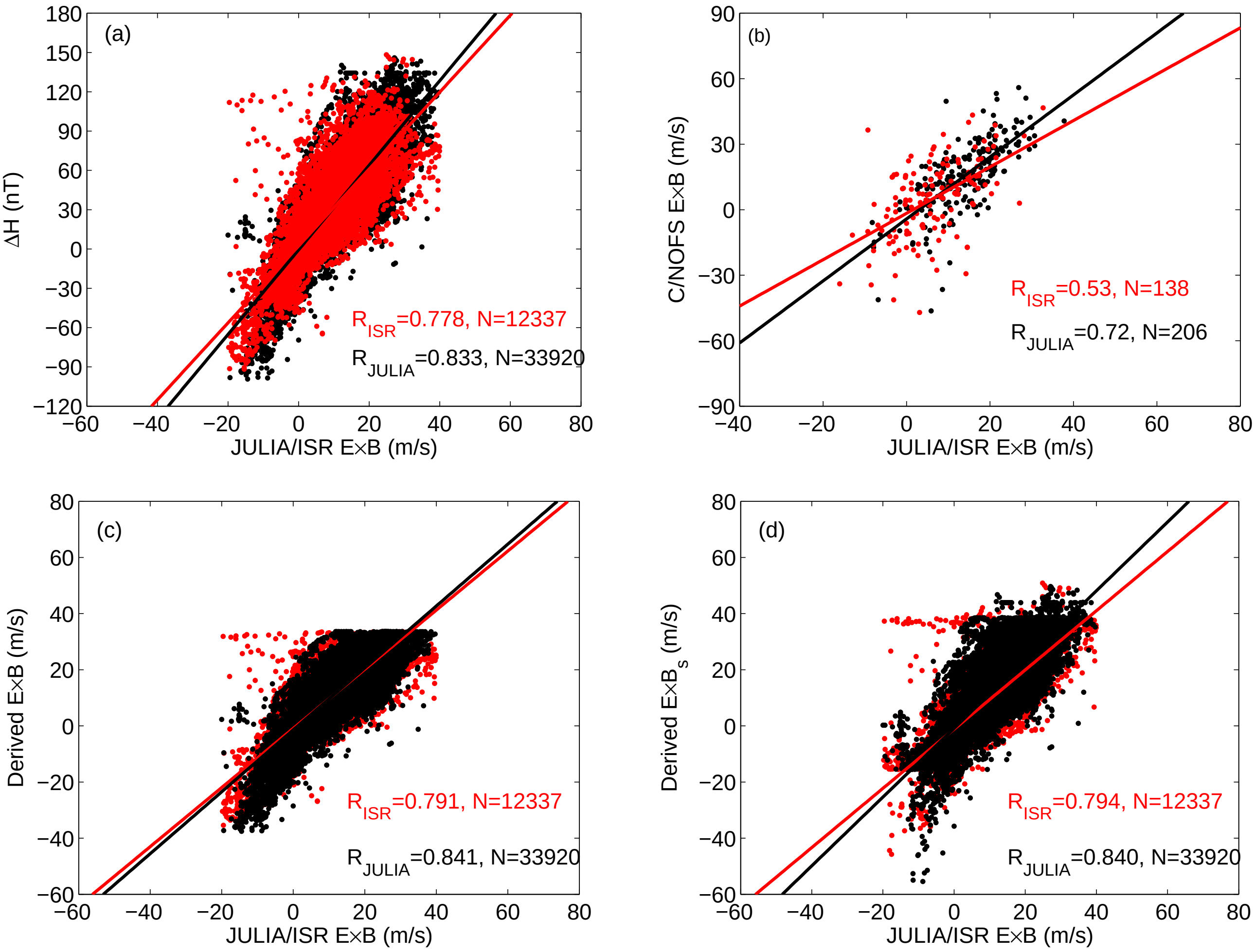

Figure 4: Scatter plots of measured (JULIA and ISR) vertical $\mathbf{E} \times \mathbf{B}$ drift and (a) ΔH, (b) C/NOFS vertical $\mathbf{E} \times \mathbf{B}$, (c) derived vertical $\mathbf{E} \times \mathbf{B}$ drift using equations (1), (d) derived vertical $\mathbf{E} \times \mathbf{B}$ drift using equations (2 and 3).

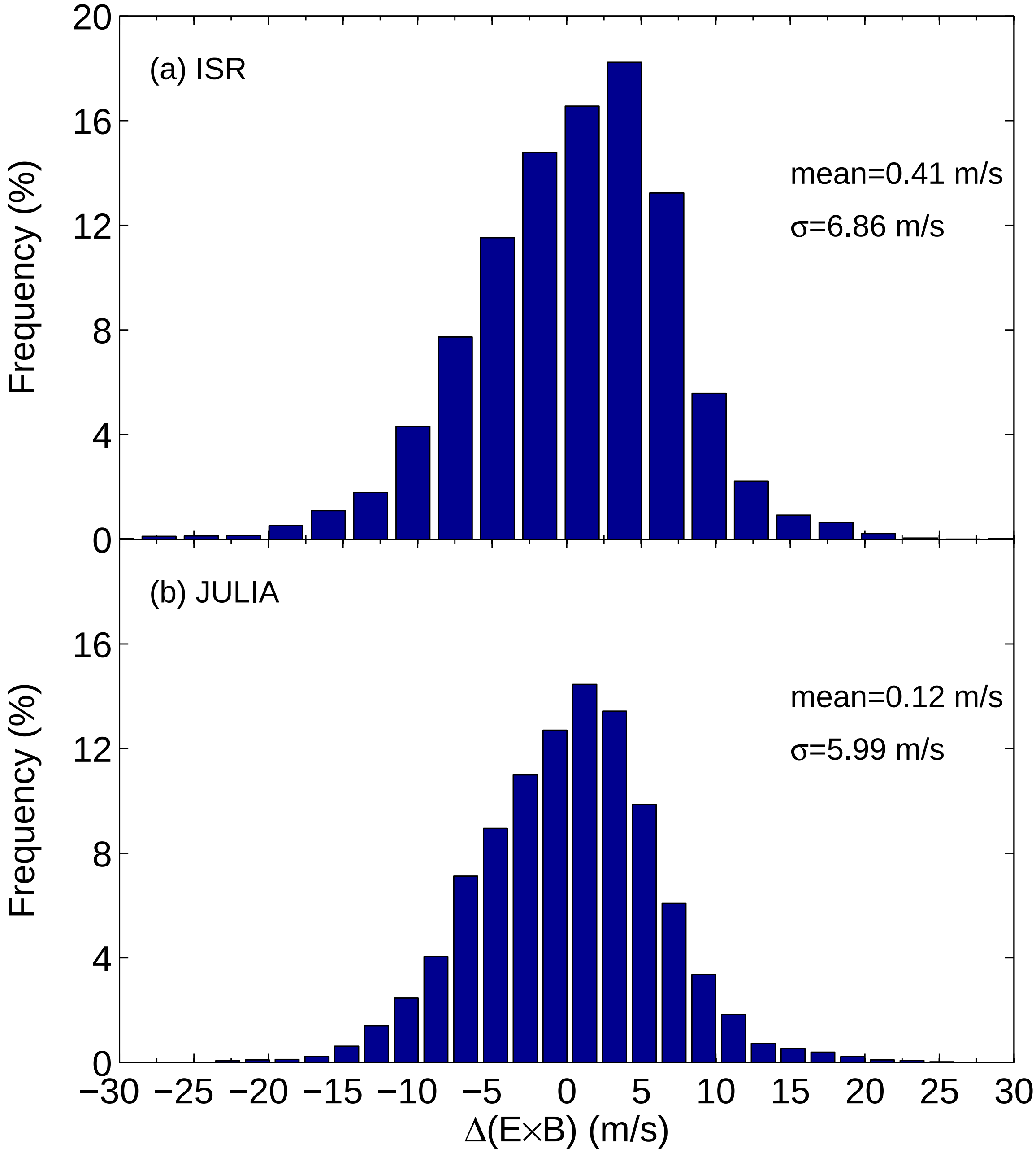

Figure 5: Distribution of differences (observed-derived=$\Delta(\mathbf{E} \times \mathbf{B})$) between derived and observed (a) ISR, and (b)JULIA vertical $\mathbf{E} \times \mathbf{B}$ drifts during for 2008-2014.

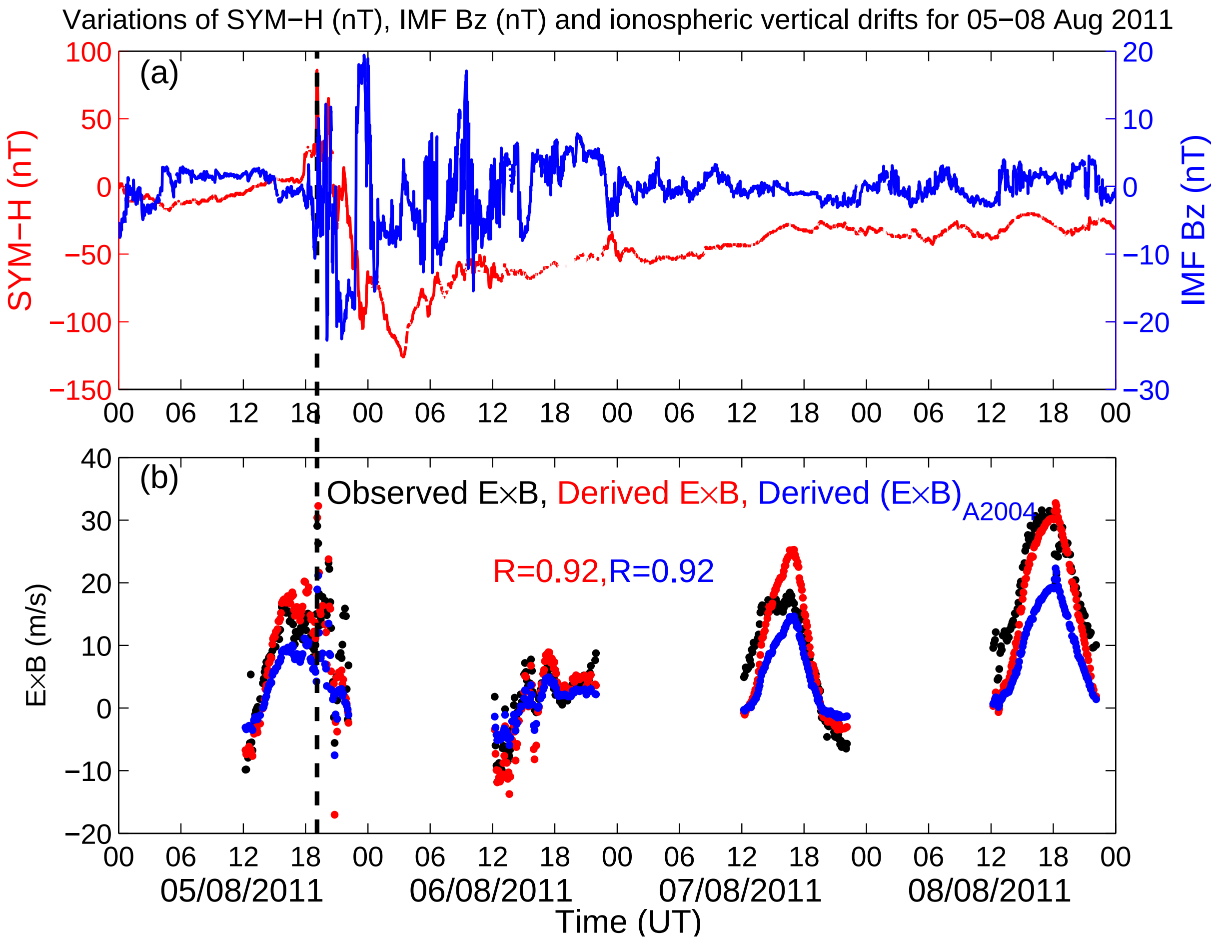

Figure 6: Changes in (a) SYM-H (nT) and IMF Bz (nT) for 05-08 August 2011 storm period, (b) ISR observed (black dots) and derived vertical $\mathbf{E} \times \mathbf{B}$ (m/s) with C/NOFS (red dots) and JULIA (blue dots denoted as $(\mathbf{E} \times \mathbf{B})_{\mathbf{A2004}}$ obtained using expression developed by Anderson et al., [2004]) based functions during the storm period of 05-08 August 2011. The vertical dashed line represents the storm onset time at 1906 UT on 05 August 2011. Jicamarca LT=UT-5.15.

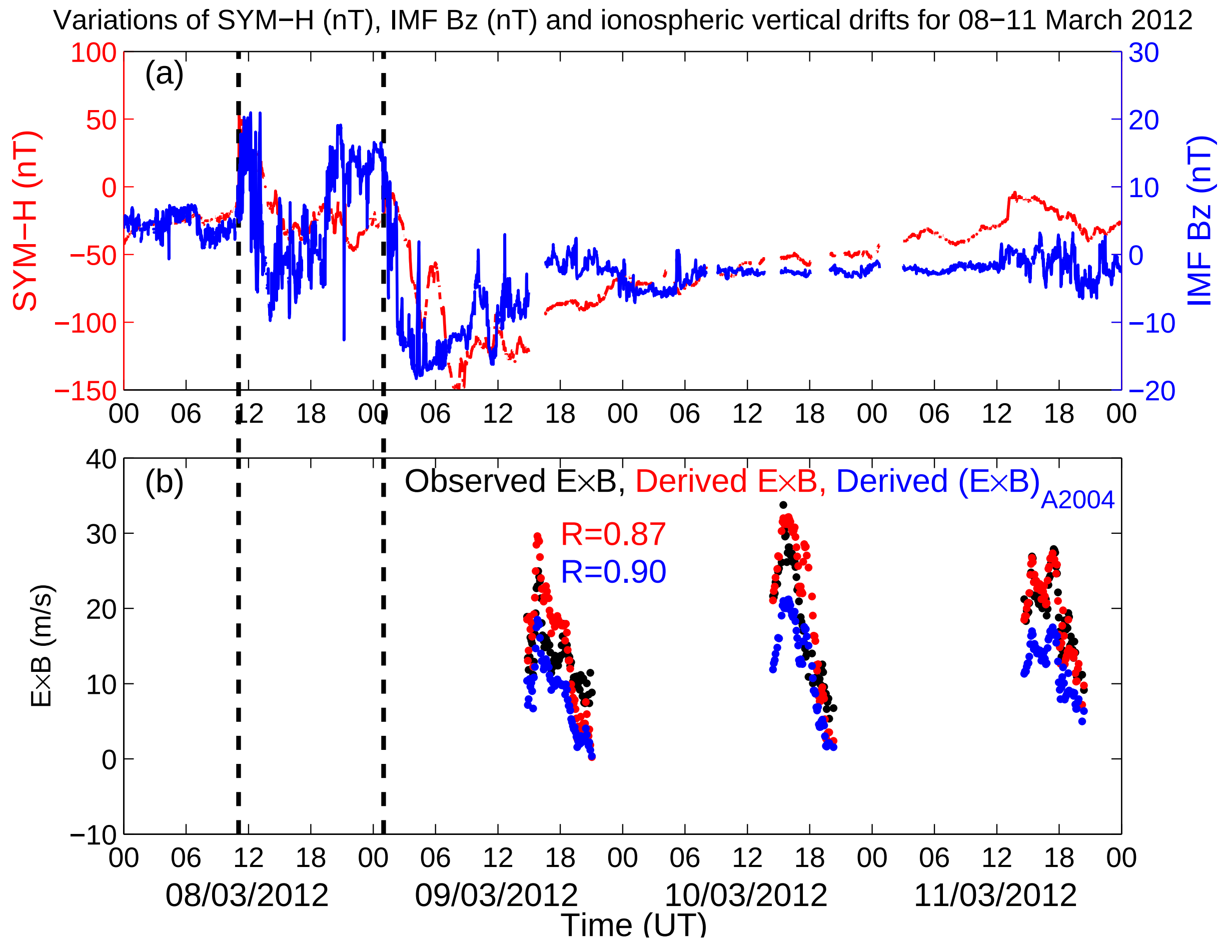

Figure 7: Variations in (a) SYM-H (nT) and IMF Bz (nT) for 08-11 March 2012 storm period, (b) JULIA observed (black dots) and derived vertical $\mathbf{E} \times \mathbf{B}$ (m/s) with C/NOFS (red dots) and JULIA (blue dots denoted as $(\mathbf{E} \times \mathbf{B})_{\mathbf{A2004}}$ obtained using expression developed by Anderson et al., [2004]) based functions during the storm period of 08-11 March 2012. Vertical dashed lines correspond to the shock and mainphase onset times at 1103 UT and 0100 UT on 08 March and 09 March respectively

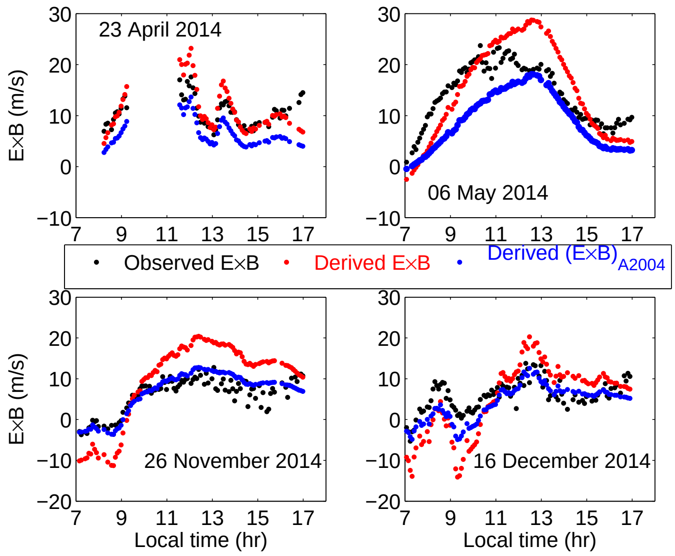

(a) ISR (black dots) and derived (red and blue dots) $\mathbf{E} \times \mathbf{B}$ (m/s) in 2014

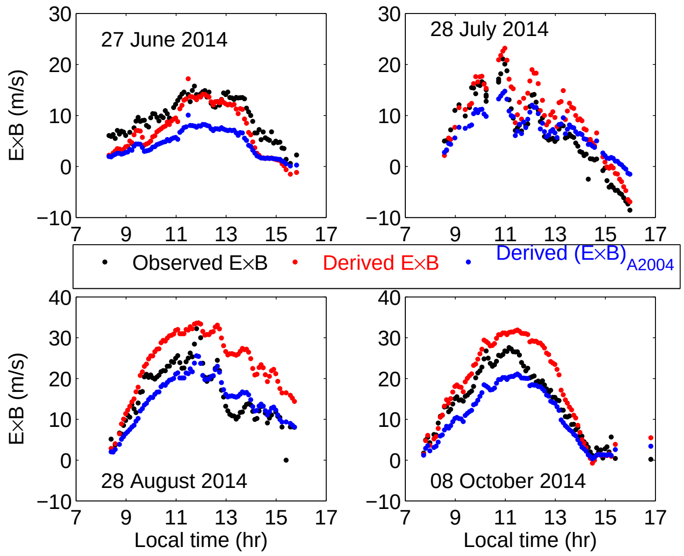

(b) JULIA (black dots) and derived (red and blue dots) $\mathbf{E} \times \mathbf{B}$ (m/s) in 2014

Figure 8: Comparison of observed ISR/JULIA (black dots) and derived vertical $\mathbf{E} \times \mathbf{B}$ (m/s) with C/NOFS (red dots) and JULIA (blue dots denoted as $(\mathbf{E} \times \mathbf{B})_{\mathbf{A2004}}$ obtained using expression developed by Anderson et al., [2004]) based functions on randomly selected days in 2014 where measured data exists. (a) and (b) represent comparisons with ISR and JULIA measurements respectively.

Figure 1.

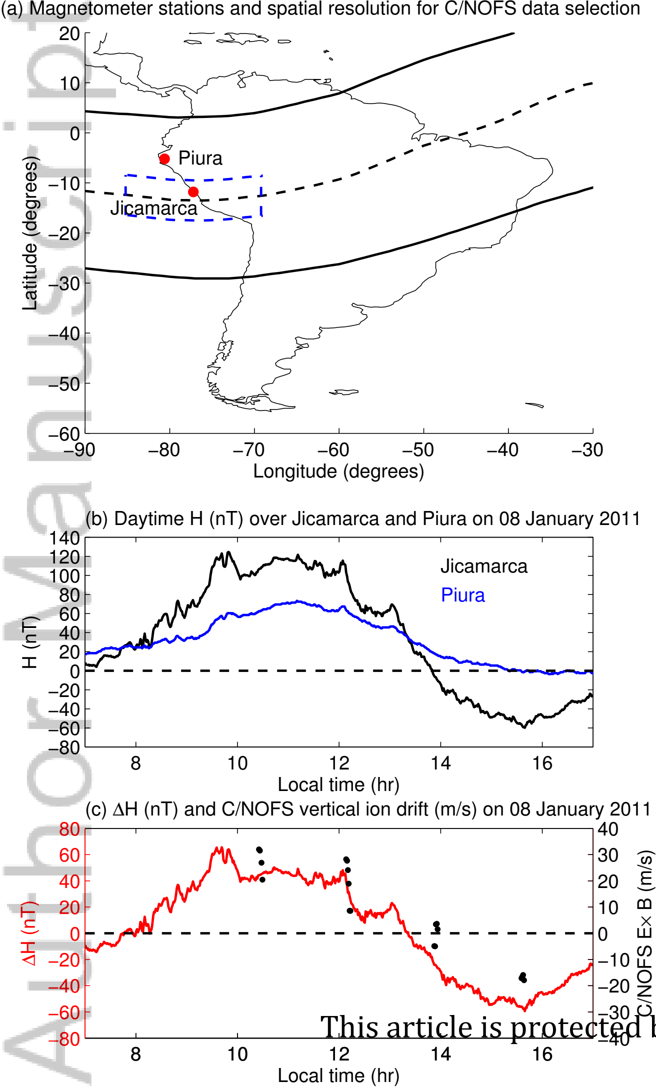
(a) Magnetometer stations and spatial resolution for C/NOFS data selection
Latitude (degrees)
Longitude (degrees)
Piura
Jicamarca
(b) Daytime H (nT) over Jicamarca and Piura on 08 January 2011
H (nT)
Local time (hr)
Jicamarca
Piura
(c) ΔH (nT) and C/NOFS vertical ion drift (m/s) on 08 January 2011
ΔH (nT)
C/NOFS E× B (m/s)
Local time (hr)

Figure 2.

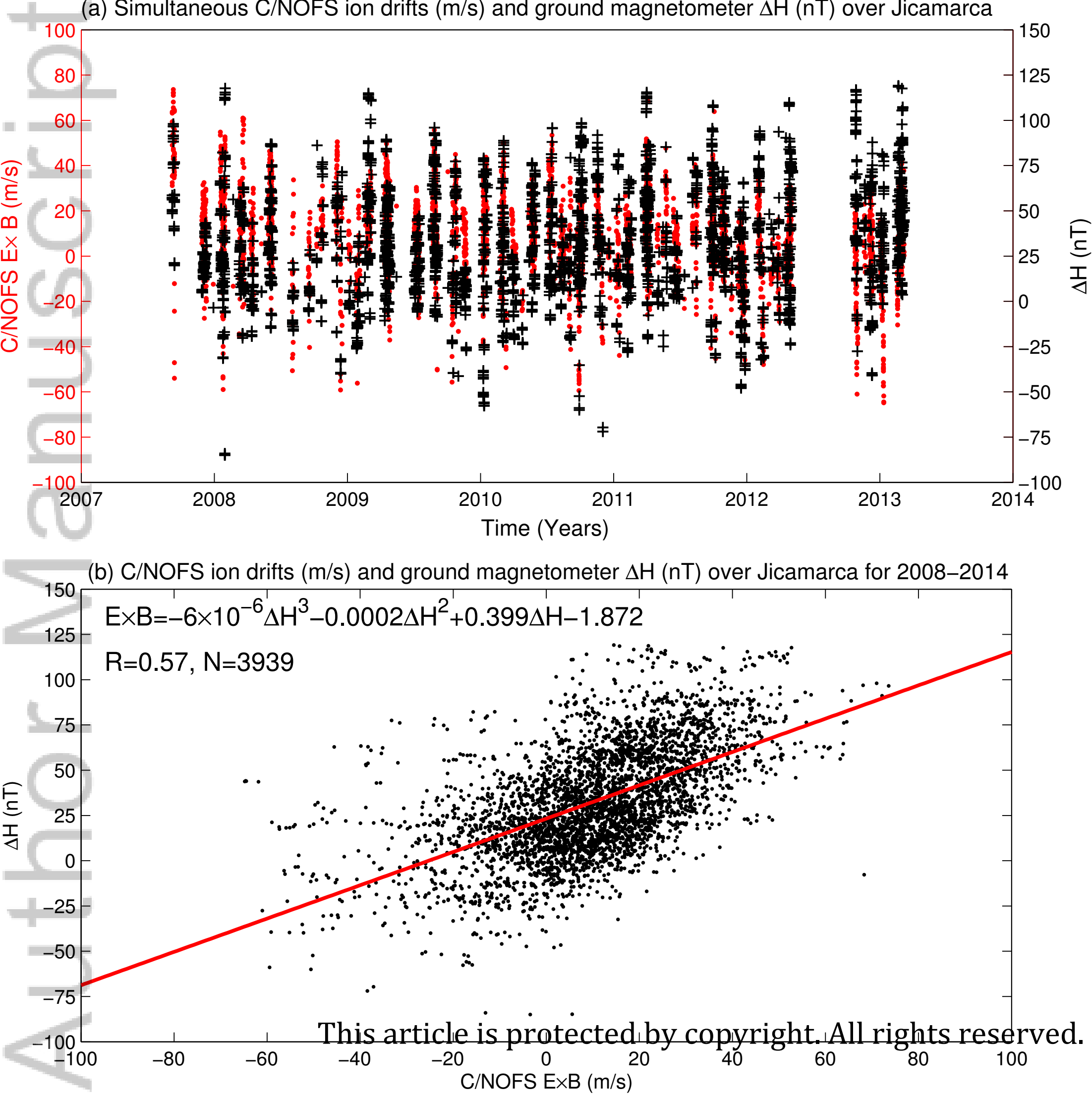

(a) Simultaneous C/NOFS ion drifts (m/s) and ground magnetometer ΔH (nT) over Jicamarca
C/NOFS E× B (m/s)
ΔH (nT)
Time (Years)
(b) C/NOFS ion drifts (m/s) and ground magnetometer ΔH (nT) over Jicamarca for 2008–2014
E×B=–6×10^−6ΔH^3–0.0002ΔH^2+0.399ΔH–1.872
R=0.57, N=3939
ΔH (nT)
C/NOFS E×B (m/s)

Figure 3.

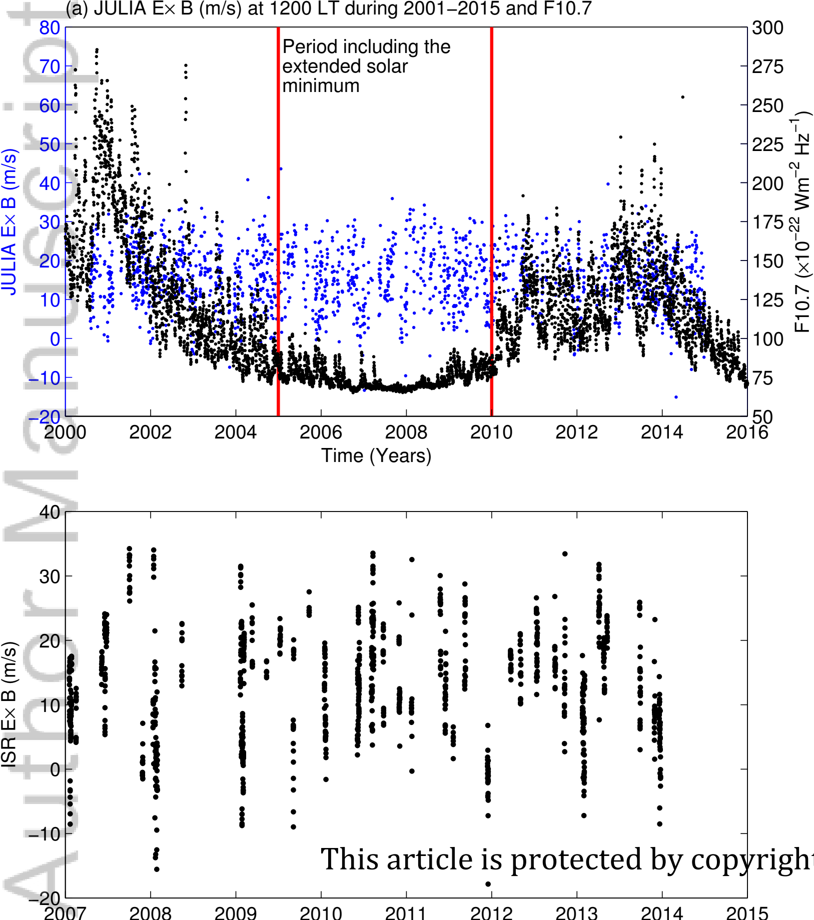
(a) JULIA E× B (m/s) at 1200 LT during 2001–2015 and F10.7
Period including the extended solar minimum
JULIA E× B (m/s)
F10.7 (×10^{-22} Wm^{-2} Hz^{-1})
Time (Years)
ISR E× B (m/s)
80
70
60
50
40
30
20
10
0
−10
−20
300
275
250
225
200
175
150
125
100
75
50
2000
2002
2004
2006
2008
2010
2012
2014
2016
40
30
20
10
0
−10
−20
2007
2008
2009
2010
2011
2012
2013
2014
2015

Figure 4.

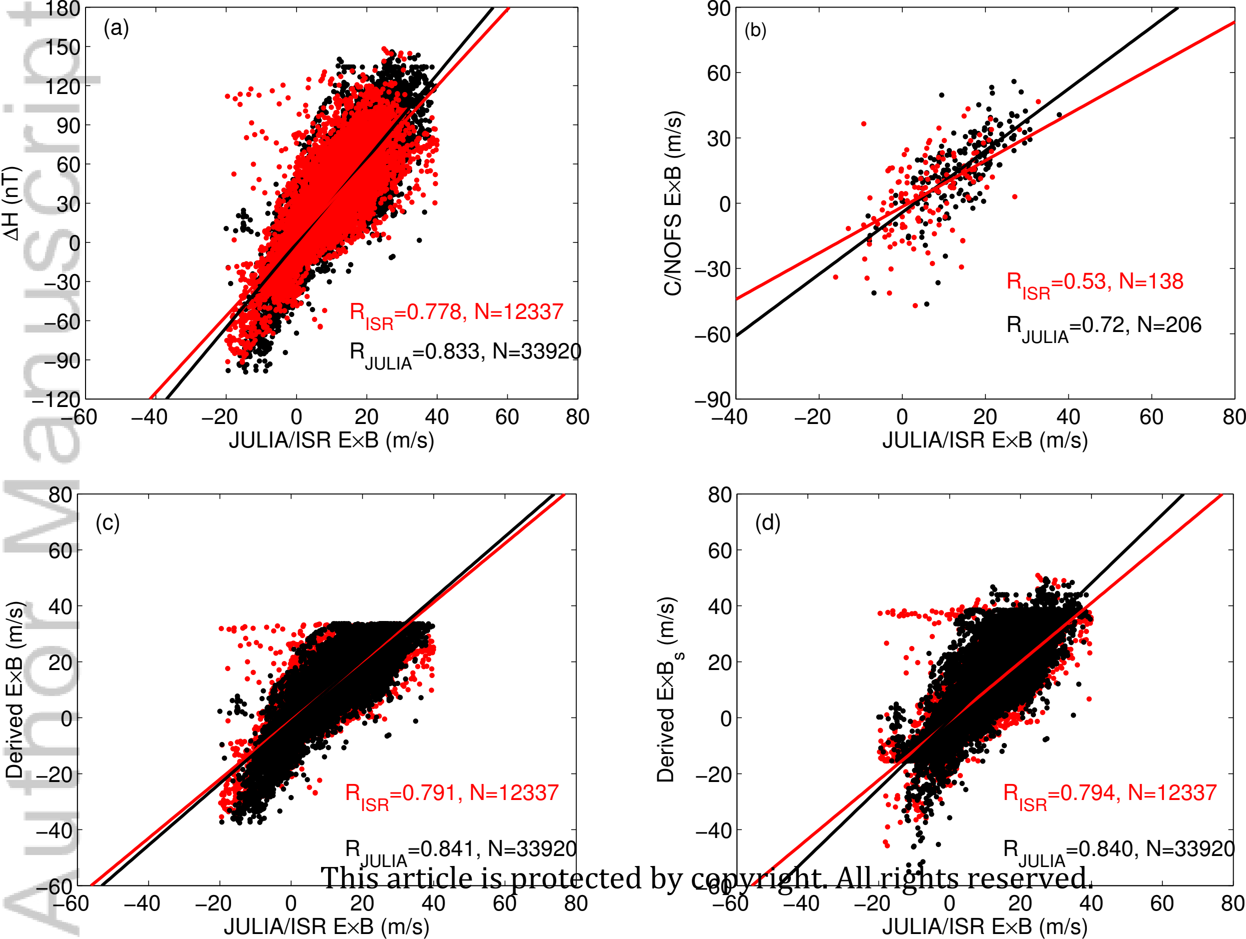
(a)
ΔH (nT)
JULIA/ISR E×B (m/s)
R_ISR=0.778, N=12337
R_JULIA=0.833, N=33920
(b)
C/NOFS E×B (m/s)
JULIA/ISR E×B (m/s)
R_ISR=0.53, N=138
R_JULIA=0.72, N=206
(c)
Derived E×B (m/s)
JULIA/ISR E×B (m/s)
R_ISR=0.791, N=12337
R_JULIA=0.841, N=33920
(d)
Derived E×B_s (m/s)
JULIA/ISR E×B (m/s)
R_ISR=0.794, N=12337
R_JULIA=0.840, N=33920

Figure 5.

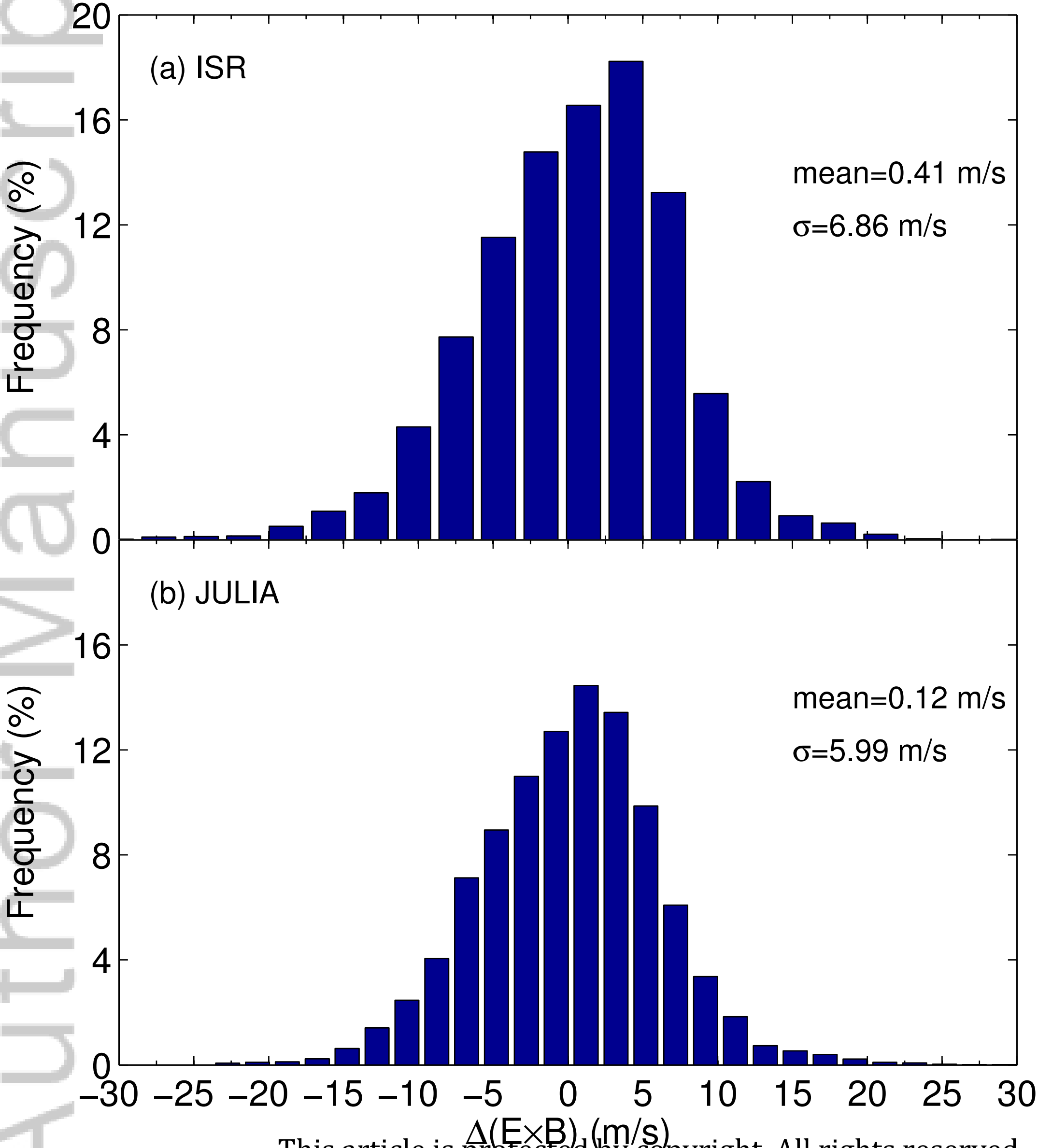
(a) ISR
mean=0.41 m/s
σ=6.86 m/s
Frequency (%)
(b) JULIA
mean=0.12 m/s
σ=5.99 m/s
Frequency (%)
0
4
8
12
16
20
−30
−25
−20
−15
−10
−5
0
5
10
15
20
25
30
Δ(E×B) (m/s)

Figure 6.

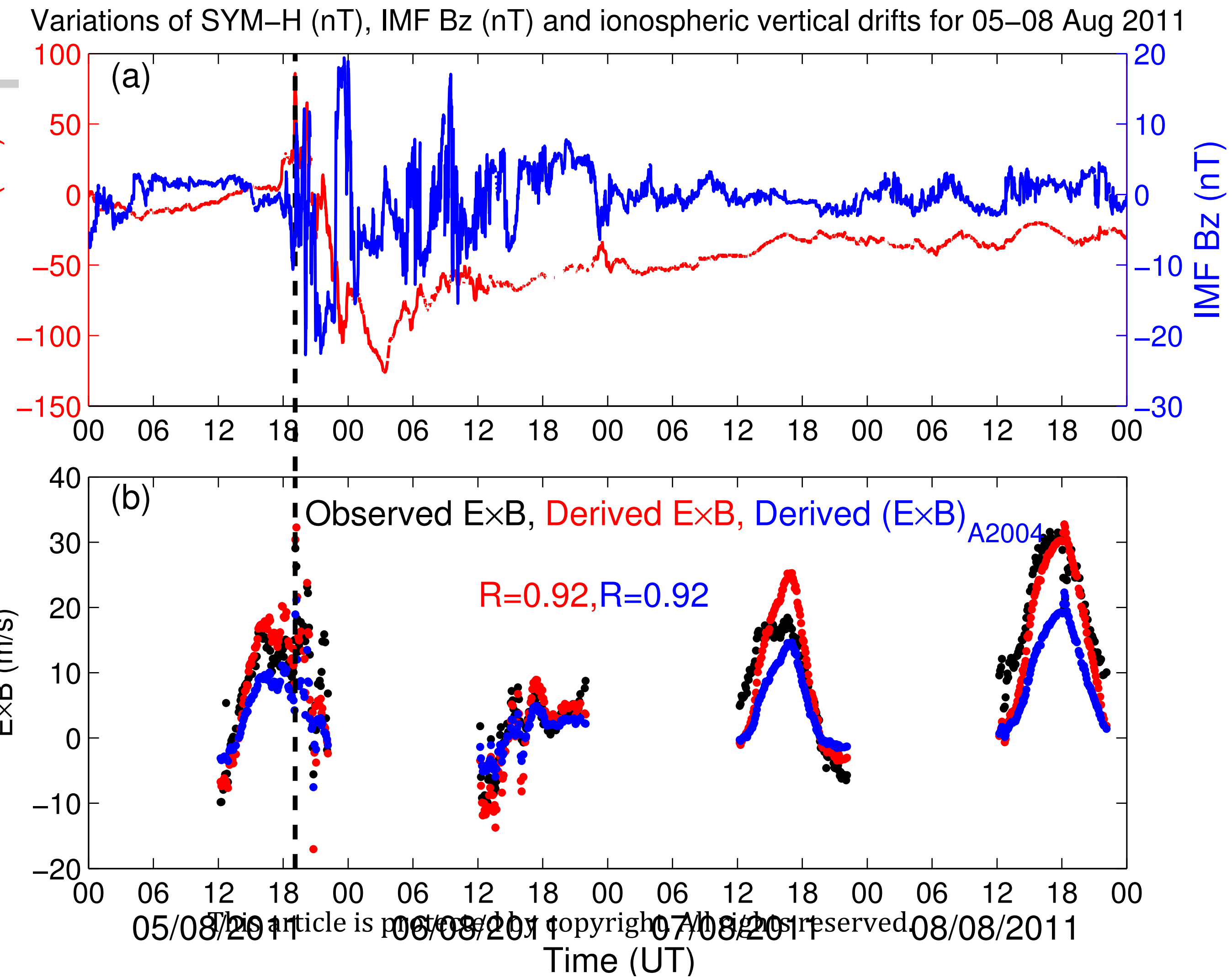

Variations of SYM−H (nT), IMF Bz (nT) and ionospheric vertical drifts for 05−08 Aug 2011
(a)
SYM−H (nT)
IMF Bz (nT)
(b)
Observed E×B, Derived E×B, Derived (E×B)A2004
R=0.92,R=0.92
E×B (m/s)
05/08/2011
06/08/2011
07/08/2011
08/08/2011
Time (UT)

Figure 7.

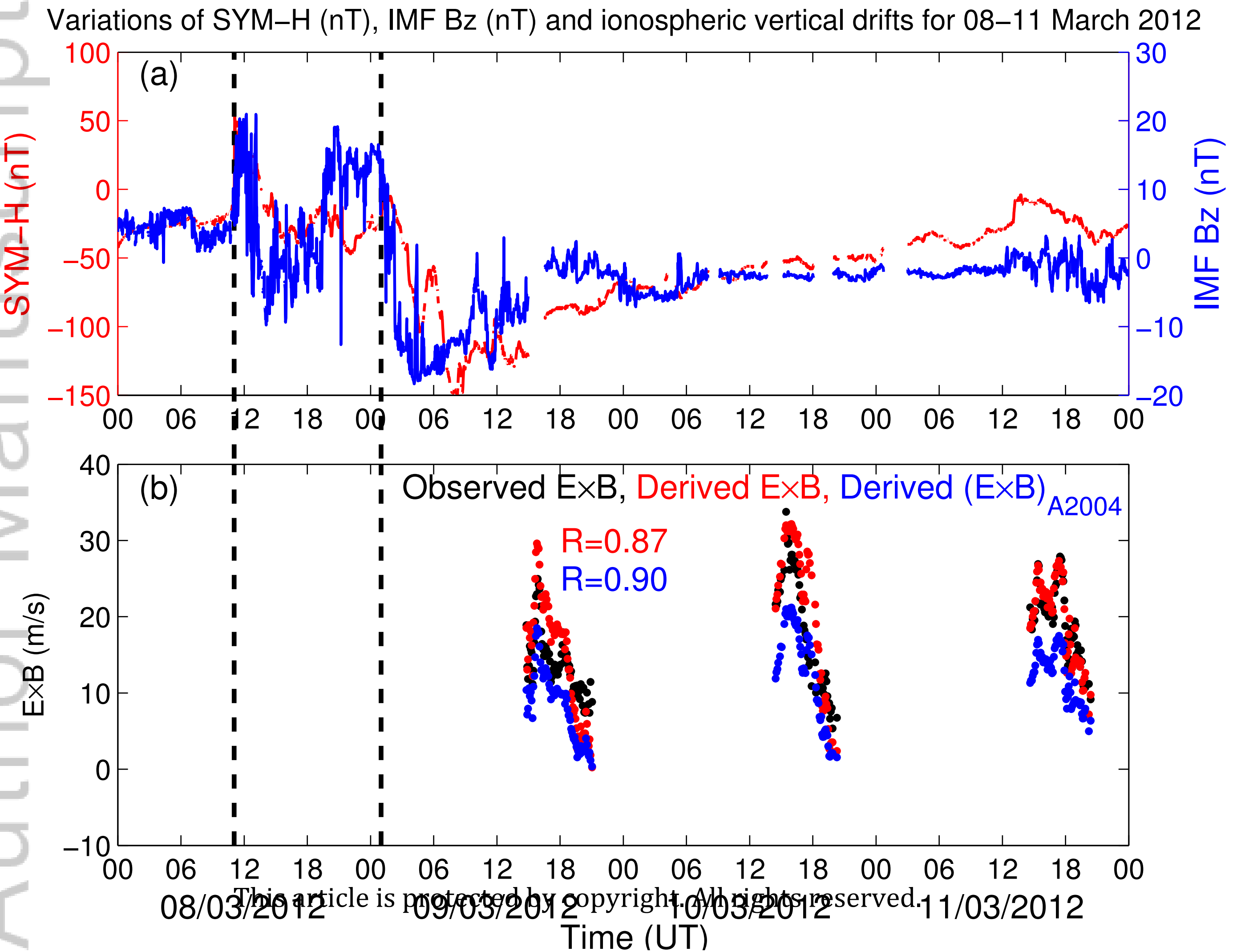
Variations of SYM−H (nT), IMF Bz (nT) and ionospheric vertical drifts for 08−11 March 2012
(a)
SYM−H (nT)
IMF Bz (nT)
100
50
0
−50
−100
−150
30
20
10
0
−10
−20
00
06
12
18
(b)
Observed E×B, Derived E×B, Derived (E×B)A2004
R=0.87
R=0.90
E×B (m/s)
40
30
20
10
0
−10
08/03/2012
09/03/2012
10/03/2012
11/03/2012
Time (UT)

Figure 8.

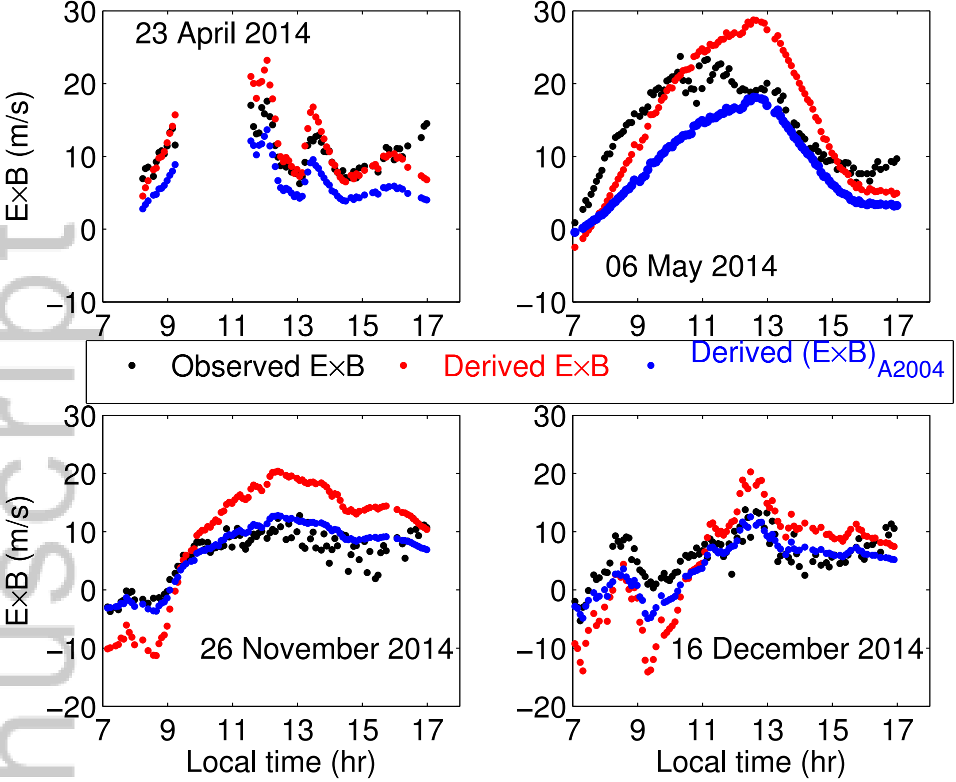

(a) ISR (black dots) and derived (red and blue dots) $\mathbf{E} \times \mathbf{B}$ (m/s) in 2014

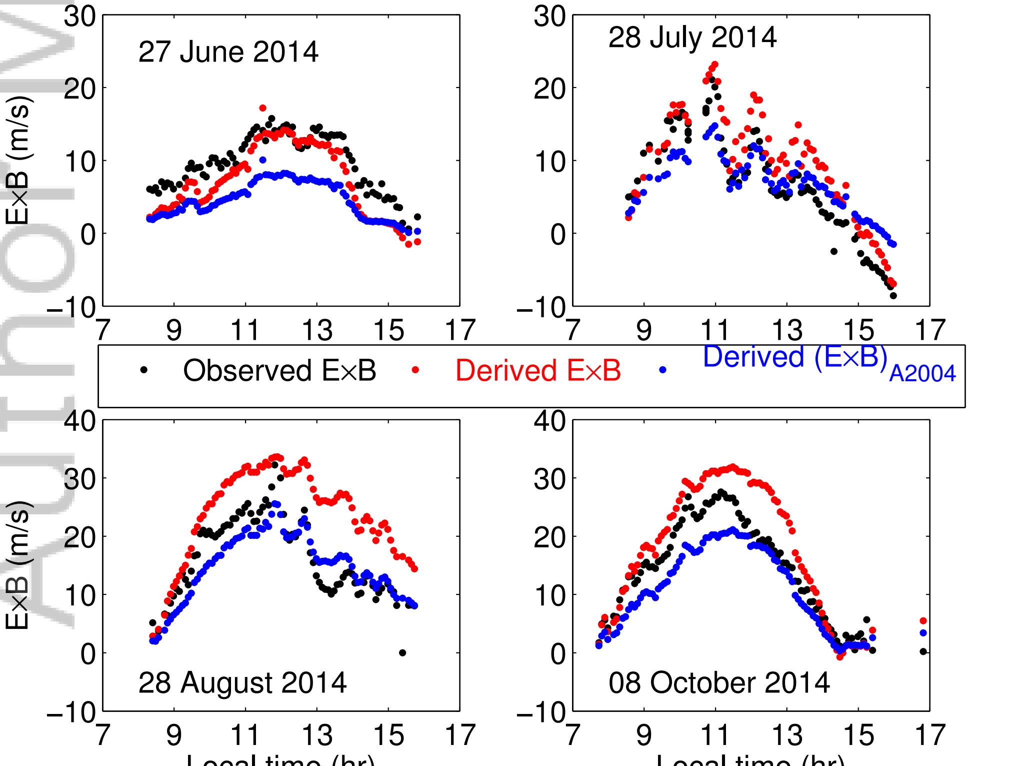

(b) JULIA (black dots) and derived (red and blue dots) $\mathbf{E} \times \mathbf{B}$ (m/s) in 2014

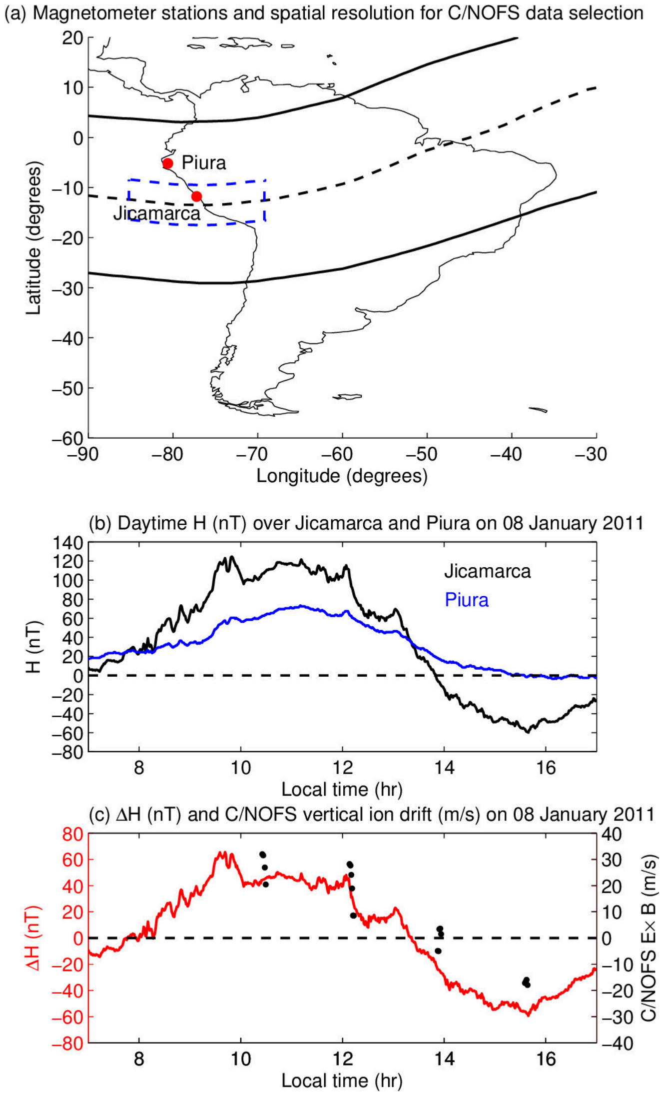

2018ja025685-f02-z-.eps

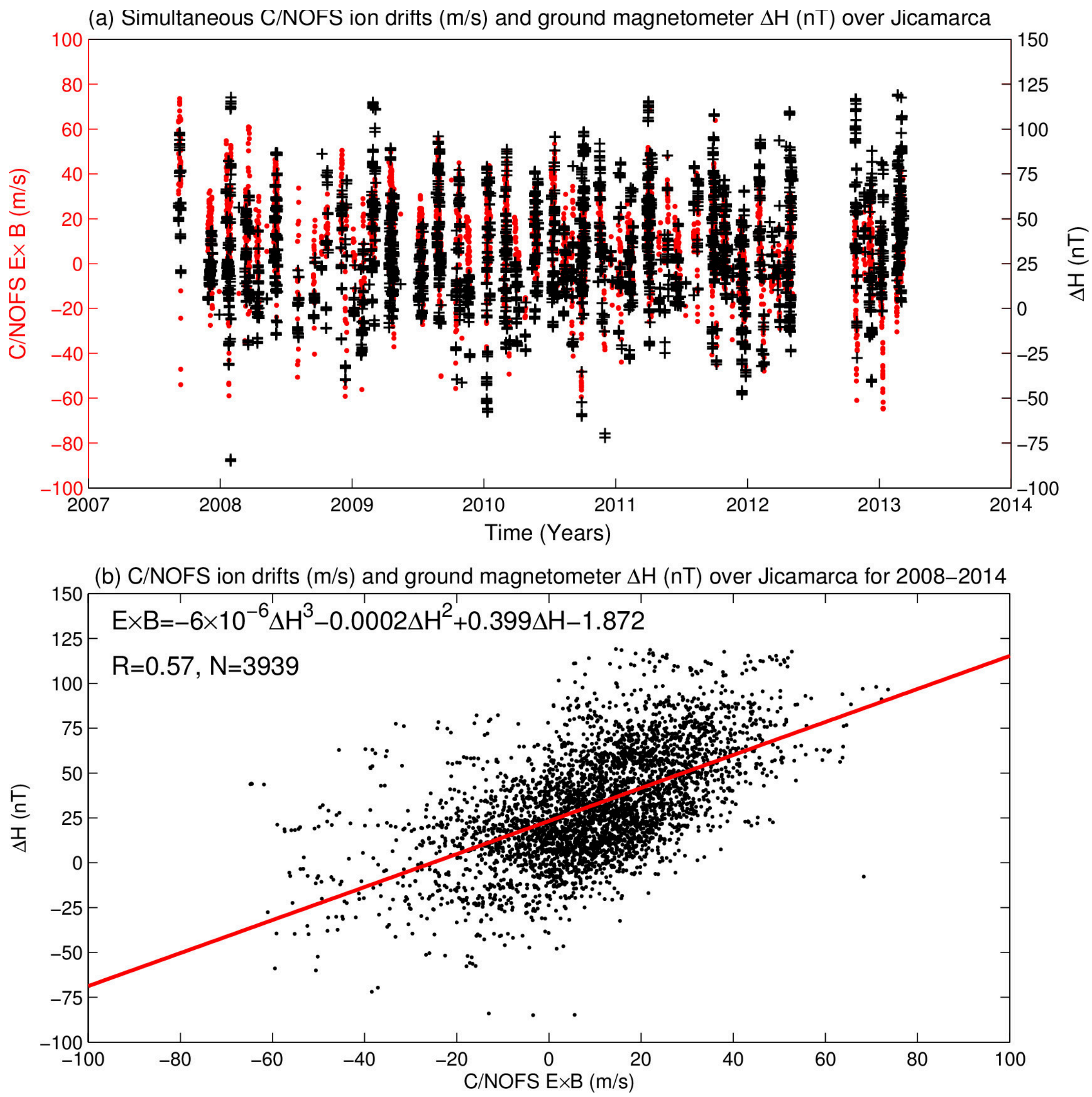

2018ja025685-f03-z-.eps

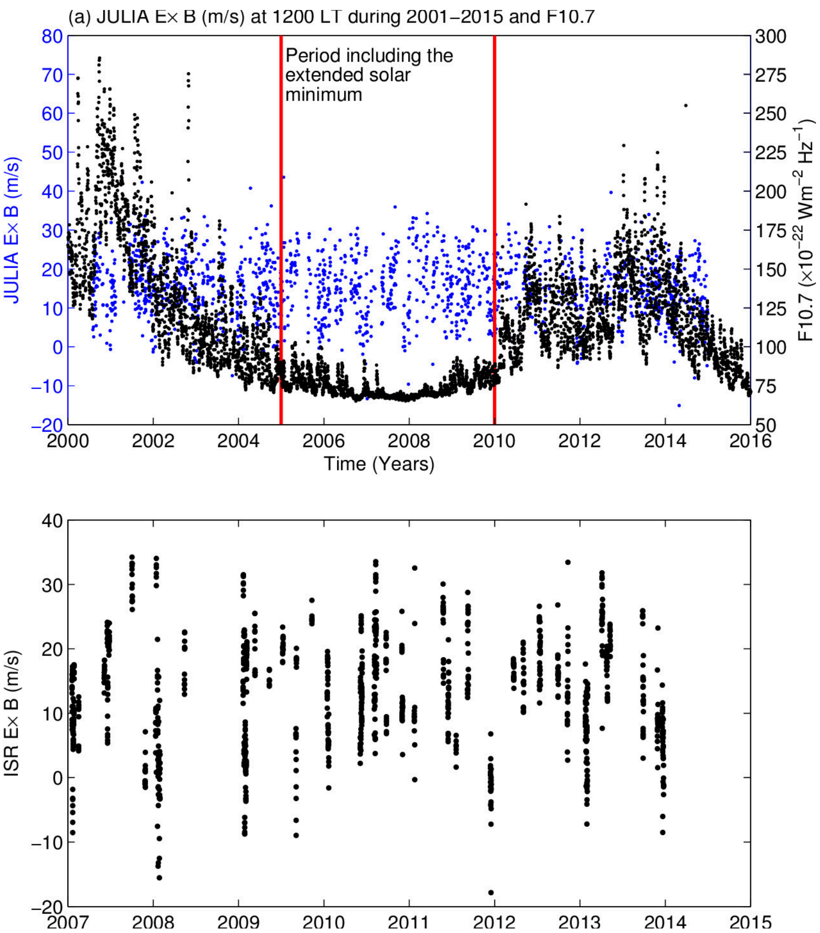

2018ja025685-f04-z-.eps

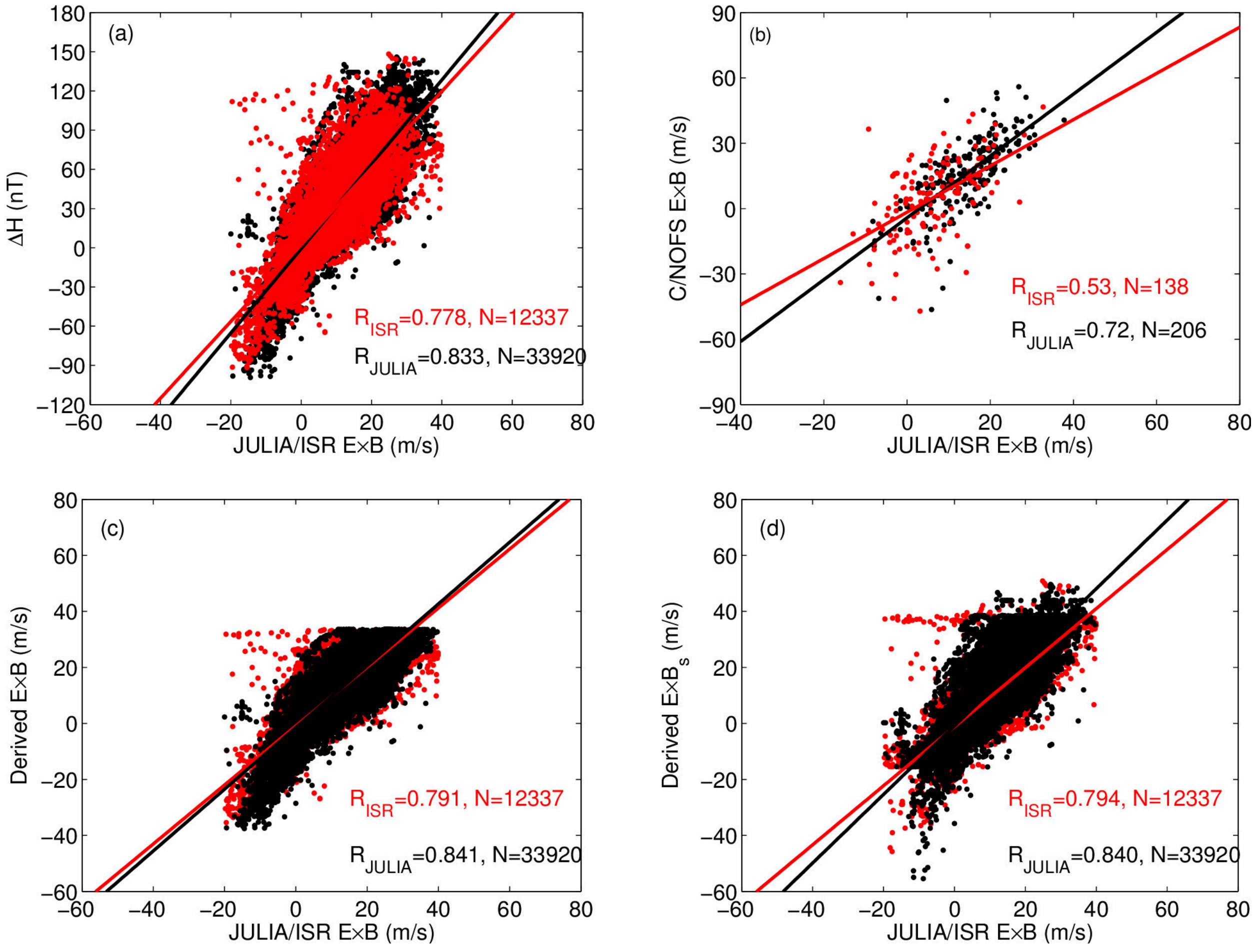

2018ja025685-f05-z-.eps

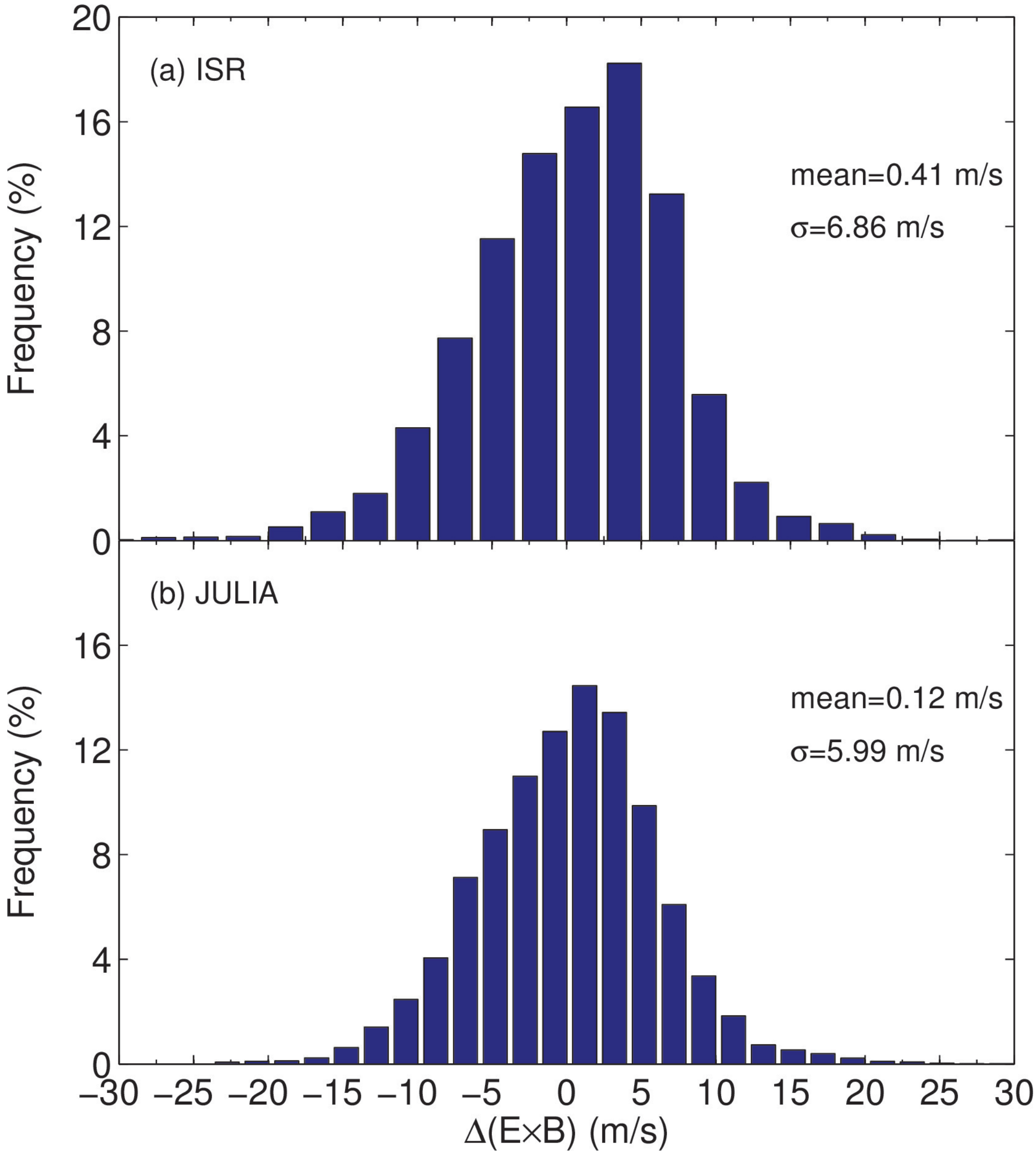

2018ja025685-f06-z-.eps

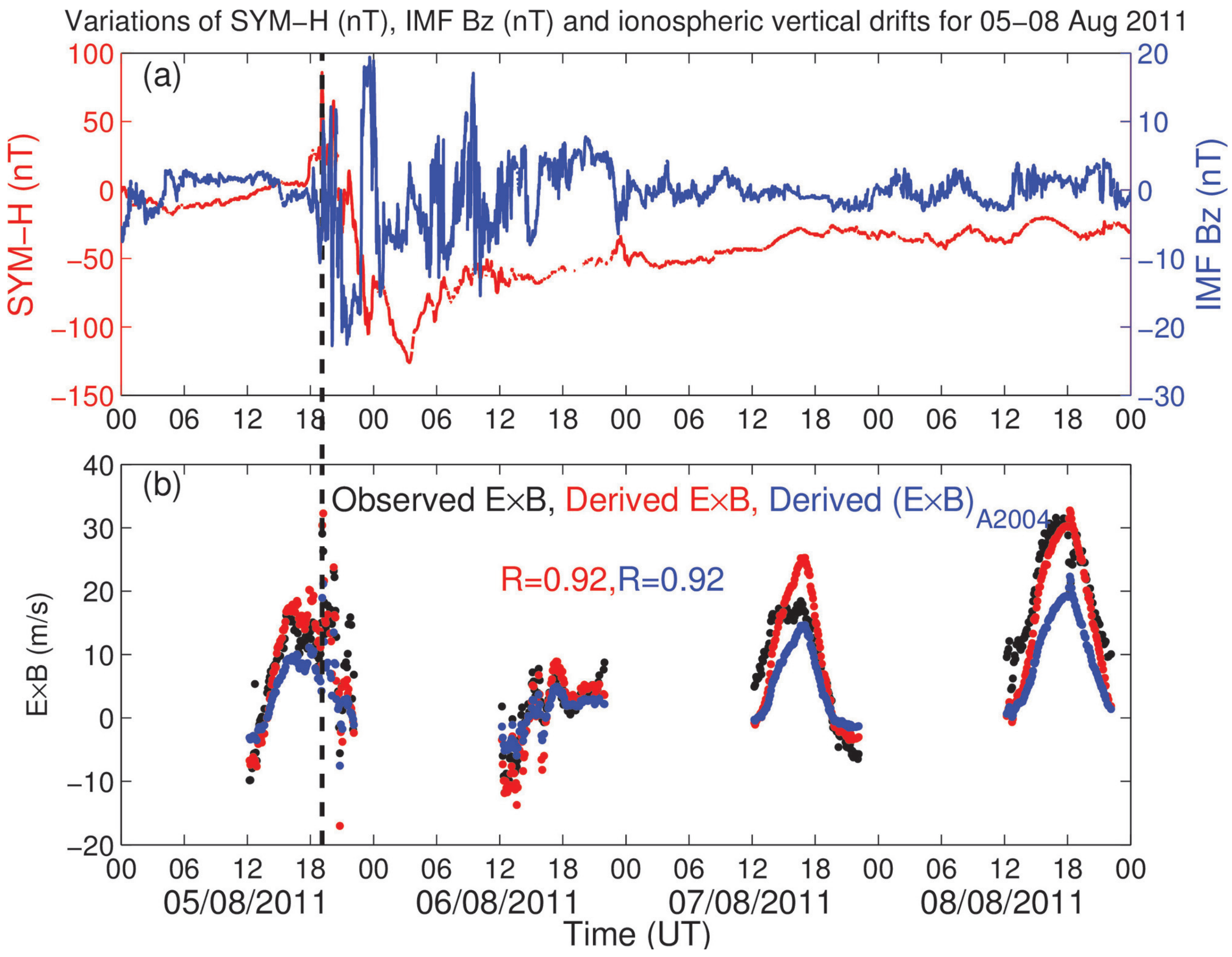

2018ja025685-f07-z-.eps

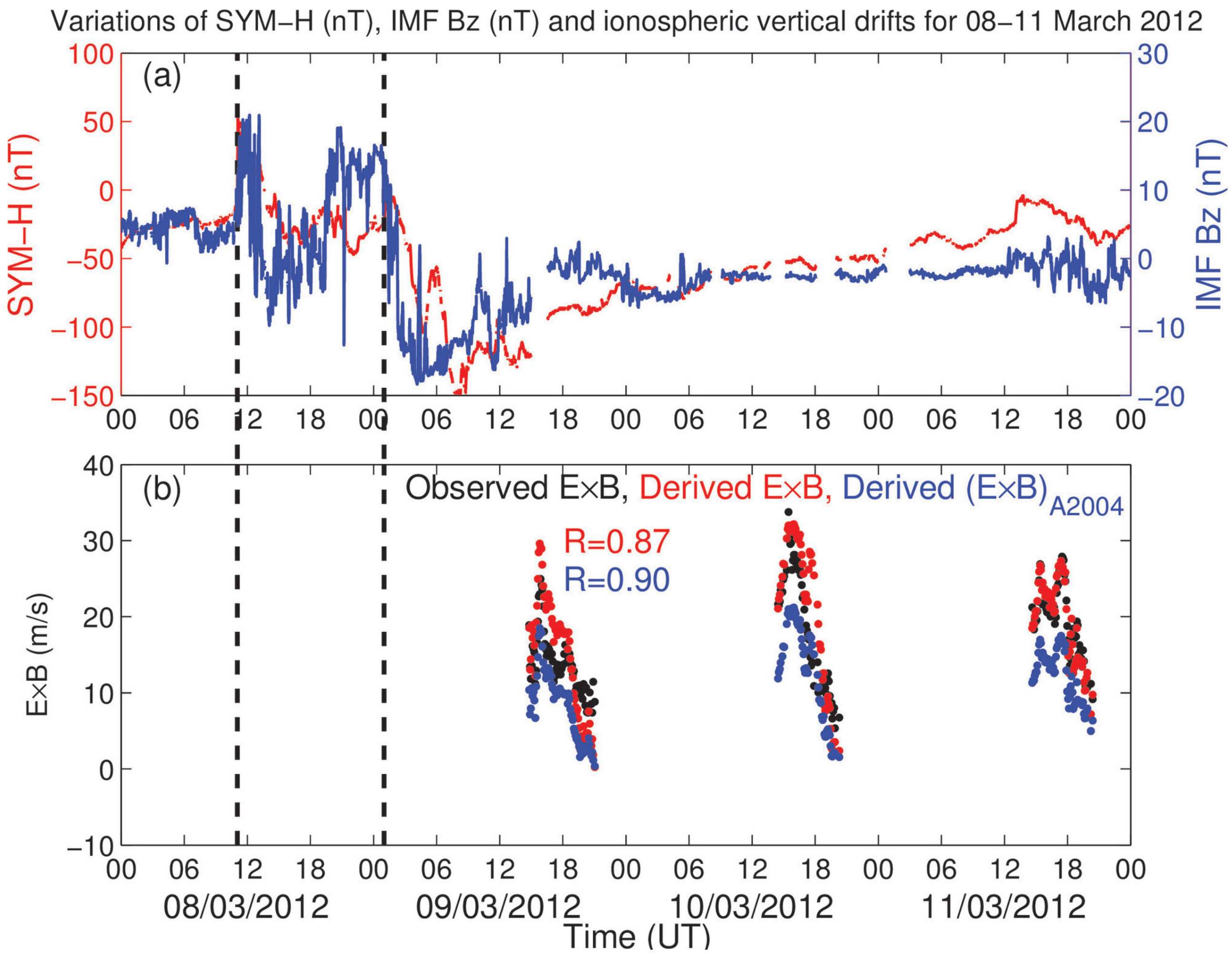

2018ja025685-f08-z-.eps

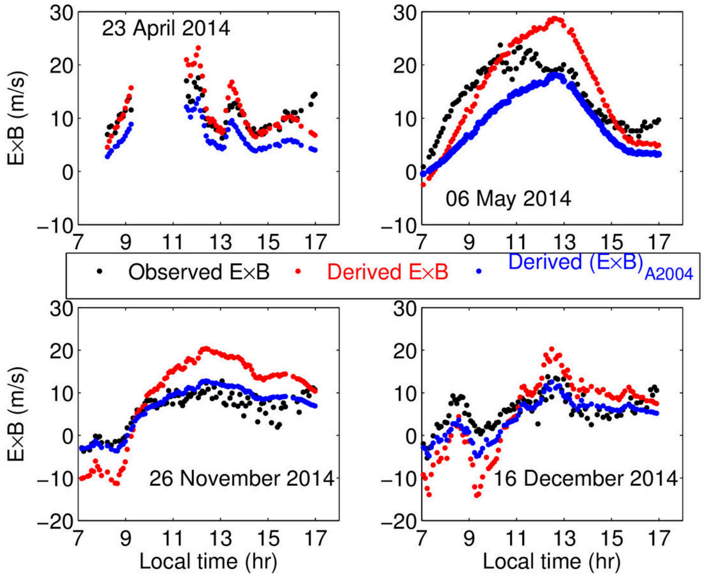

(a) ISR (black dots) and derived (red and blue dots) $\mathbf{E} \times \mathbf{B}$ (m/s) in 2014

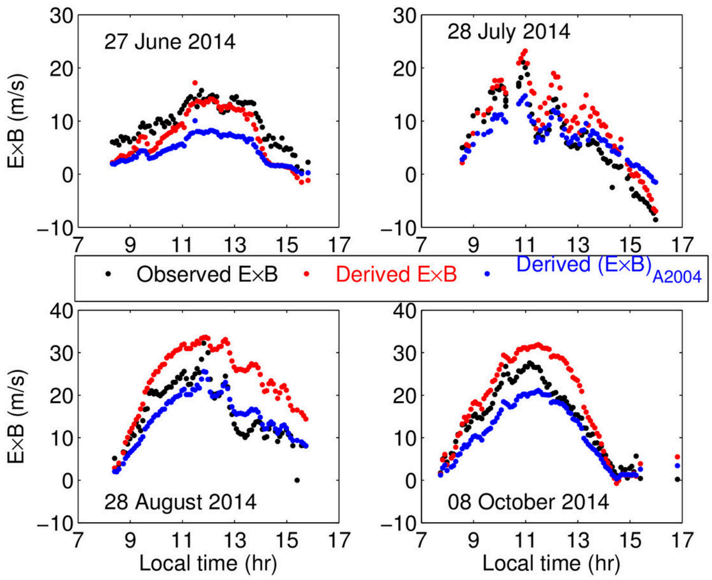

(b) JULIA (black dots) and derived (red and blue dots) $\mathbf{E} \times \mathbf{B}$ (m/s) in 2014

2018ja025685-f09-z-.eps